ADDIS ABABA UNIVERSITY

DEPARTMENT OF EARTH SCIENCES

SCHOOL OF GRADUATE STUDIES

GEOLOGICAL FACTORS GOVERNING the VULNERABILITY of LAND to DEGRADATION: - *the case of HOSAINA – WERABE AREA*, USING REMOTE SENSING and GIS

BY

MEERAPH HABTEWOLD

JULY 2006

GEOLOGICAL FACTORS GOVERNING the VULNERABILITY of LAND to DEGRADATION: - *the case of HOSAINA – WERABE AREA*, USING REMOTE SENSING and GIS

A THESIS PRESENTED TO

THE SCHOOL OF GRADUATE STUDIES OF

ADDIS ABABA UNIVERSITY

In partial Fulfillment of the requirements for the Degree

Master of Science in Remote Sensing and GIS

BY

MEERAPH HABTEWOLD

JULY 2006

ADDIS ABABA UNIVERSITY

SCHOOL OF GRADUATE STUDIES

GEOLOGICAL FACTORS GOVERNING the VULNERABILITY of LAND to DEGRADATION: - *the case of HOSAINA – WERABE AREA*, USING REMOTE SENSING and GIS

By
MEERAPH HABTEWOLD

Faculty of Natural Science
Department of Earth Sciences
Remote sensing and GIS

Approval By Board of Examiners

Dr. Dereje Ayalew _____
Chairman, Department
Graduate Committee

Dr. Mohammed Umer _____
Advisor

Dr. Asfawossen Asrat _____
Advisor

Dr. Dagnachew legesse _____
Examiner

Dr. K.V. Suryabhagavan _____
Examiner

Declaration

I, the under signed, declare that this thesis is my work and that all sources of material used for the thesis have been dully acknowledged.

Name: Meeraph Habtewold

Signature:_____

Place and date of submission,

July 2006, Addis Ababa.

Table of Contents

Page

List of Figures v

List of Tables ix

List of Plates x

Acknowledgment xi

Abstract xiii

1. General introduction 1

1.1 Introduction 1

1.2 Objectives of the study 2

1.3 The study area 4

1.3.1 Introduction 4

1.3.2 Location, areal extent and accessibility of the study area 6

1.3.3 Topography and landforms 7

1.3.4 Soil 9

1.3.5 Drainage 10

1.3.6 Land use / Land cover 11

1.3.7 Rainfall and Temperature 12

1.3.8 Population 16

2. Land degradation problem 17

2.1 Land degradation 17

2.2 Forms of land degradation 18

2.3 Previous Works 19

3. Geology 21

3.1 Regional geology 21

3.2 Geology of the study area 23

3.2.1 Lithostratigraphy 24

3.2.2 Geological structures 25

4. Remote sensing and GIS techniques 29

4.1 Introduction 29

Materials used 30

Softwares used 31

4.2. Remote sensing analyses 32

Digital image processing 35

Preprocessing 35

Image enhancement 36

Image transformation 37

Image classification 39

4.3. GIS analyses 40

5. Assessment of land degradation: rate, areal extent and spatial variations of degradation....41

5.1 Introduction....41

5.2 Time series/ change analysis....42

5.2.1 Rate and areal extent of land degradation....42

5.2.2 Spatial variations of land degradation....47

6 Land degradation activity: assessment and GIS analyses....53

6.1 Introduction....53

6.2 Land degradation controlling factors and GIS analyses....55

6.2.1 Land degradation distribution map....55

6.2.2 Constraint data layer....56

6.2.3 Factors that control land degradation in the study area....57

Geological structures....57

Slope angle (geomorphology)....58

Drainage....59

Geology (lithology)....60

Land use/ land cover....61

Soil....64

6.3 Normalization (standardization) of factor maps....66

6.4 Weight of factor maps....70

6.5 Multi-Criteria Evaluation (MCE)....72

7 Conclusion and recommendation.....78

7.1 Conclusions.....78

7.2 Recommendations 80

8. References.....81

List of Figures

Figure #	List of Figures	Page #
Figure 1	Location map of the study area.	7
Figure 2	Elevation map of the study area (based on SRTM data of 2000 G.C.).	8
Figure 3	Digital Elevation Model of the study area (based on SRTM data of 2000 G.C.).	8
Figure 4	Soil map of the study area (from Ethio-GIS data).	9
Figure 5	Drainage map of the study area (digitized from the mosaic topographic map).	10
Figure 6	Land use/ land cover map (modified from Woody Biomass, 2003).	12
Figure 7(a)	Rainfall (in millimeter) data graph.	14
Figure 7(b)	Annual average maximum and minimum temperatures, (in degree centigrade).	15
Figure 8	Geological map of the study area (Modified after Tadesse et al., 2004).	24
Figure 9	Lithostratigraphy of the rift floor ignimbrite from two traverses during field survey.	28
Figure 10	Scanned 18 pieces of A4 size topographic map (left), and final mosaic topographic map (right).	32
Figure 11	Study area images of year 2000 G. C., false color composite of bands 432 in RGB (left) and panchromatic Band 8 (right).	34
Figure 12	The electromagnetic spectrum (Lillesand, 2000).	38

Figure 13	Typical spectral reflectance curves for three basic types of earth features (adapted from Swain and Davis, 1978, in Lillesand, 2000).	39
Figure 14	Intensely degraded areas in the study area.	42
Figure 15	Degraded area map of year 1973 G.C.	44
Figure 16	Degraded area map of year 1984 G.C.	44
Figure 17	Degraded area map of year 2000 G.C.	45
Figure 18	Raster Boolean map of degraded area (1) and non- degraded (0) of year 1973 G. C. exposed soil profile	45
Figure 19	Raster Boolean map of degraded area (1) and non- degraded (0) of year 1984 G.C.	46
Figure 20	Raster Boolean map of degraded area (1) and non- degraded (0) of year 2000 G.C.	46
Figure 21	The pair-wise overlay Boolean images of year 1984 and 1973 G.C.	48
Figure 22	The pair-wise overlay Boolean images of year 2000 and 1984 G.C.	49
Figure 23	Area calculated from classes that result from the pair- wise Boolean rasters of, year 1984 | year 1973 and year 2000 | year 1984, CROSSTAB overlay analysis.	50
Figure 24	Land degradation map of the study area.	56
Figure 25	Study area as Boolean constraint data layer.	57
Figure 26	Distance derived from geological structures.	58
Figure 27	Slope map expressed in degree.	59
Figure 28	Distance from drainage lines.	60

Figure 29	Reclassified geology data layer.	61
Figure 30	Land use / land cover raster map of the study area.	63
Figure 31	Reclassified land use/ land cover map of the study area (Based on the size of degraded lands in % of each land use/ land cover class).	63
Figure 32	Raster soil map of the study area.	65
Figure 33	Reclassified soil map of the study area (Based on the size of degraded lands in (%) of each soil class).	65
Figure 34	Data layer that shows proximity to geological structures.	67
Figure 35	Standardized slope data layer.	68
Figure 36	Data layer that shows proximity to drainage lines.	68
Figure 37	Standardized land use/ land cover data layer.	69
Figure 38	Standardized geology data layer.	69
Figure 39	Standardized soil data layer.	70
Figure 40	Weight of factors that control land degradation process in the study area: the pair-wise ratio matrix (left), the module result of the eigenvector of ratio matrix that gives weight for each factor (right).	72
Figure 41 (a & b)	Factors and constraint data layer (left) and their weighted linear combination result of Land degradation susceptibility map of the study area (the legend represent; high (273 and green) to low (0 and black) susceptible to land degradation activity).	73
Figure 42	Land degradation vulnerability map of the study area. Class 1(green), class 2 (blue) and class 3 (yellow) represent low, moderate and highly vulnerable areas to land degradation	74

activity respectively.

Figure 43 Weight of factors that control land degradation process in the study area taking geological structure data layer as a dominant factor: the pairwise ratio matrix (left), the module result of the eigenvector of ratio matrix that gives weight for each factor (right). 75

Figure 44 Land degradation susceptibility map that are taken geological structure as a dominant factor. 75

Figure 45 Land degradation vulnerability map that are taken geological structure as a dominant factor. 76

List of Tables

Table #	List of Tables	Page #
Table 1	Topographic sheets that were used for this study.	30
Table 2	Areas of the three years degraded and non-degraded lands and area in percent of degraded areas from the total sample site.	47
Table 3	Classes that result from the pair-wise Boolean rasters of later year / earlier year, CROSSTAB overlay analysis.	48
Table 4	Area calculated from classes that result from the pair- wise Boolean rasters of, year 1984 | year 1973, CROSSTAB overlay analysis.	49
Table 5	Area calculated from classes that result from the pair- wise Boolean rasters of year 2000 | year 1984, CROSSTAB overlay analysis.	50
Table 6	Method used for the reclassification of land use/ land cover data layer based of the study area on the amount of degraded land in % of each land use/ land cover class.	62
Table 7	Method used for the reclassification of soil data layer based of the study area on the amount of degraded land in % of each soil class.	64
Table 8	Pair-wise comparison, 9-point continuous rating scale (adapted from Saaty, 1980, in Malczewski, 1999).	71

List of Plates

Plate #	List of Plates	Page #
Plate 1	Land degradation features in the study area.	4
Plate 2	Different erosion features, those manifesting the existence of intense land degradation in the study area.	5
Plate 3	Different layers exposed by land degradation.	26
Plates (a &b)	Ignimbrite and ash layers exposed by land degradation process.	26
Plate 5	Pumice layer.	27
Plate 6	Drainage focus and follows geological structure and initiate rills or gullys on the Ignimbrite, which finally leads to the formation of inselbergs or badlands.	27

Acknowledgment

I would like to take this opportunity to give a credit to all that had made contributions to the success of my work.

I am very much honored to be the recipient of the DAAD (Deutscher Akademischer Austausch Dienst or German Academic Exchange Service) scholarship award for gave me a financial support.

I am indebted to my advisor Dr Mohammed Umer who has made contributions from the very beginning of this work and who facilitated my field trips, and for providing various materials for the study. He was also willing to help me and encourage me to accomplish this research.

I am gratefully to my advisor Dr Asfawossen Asrat who gave constructive comments during various stages of the thesis work. I benefited and learned much from the ideas he offered. I am also grateful for his guidance and assistance during fieldwork and for providing his field equipments. The photographs in the thesis are courtesy to him.

I want to thank the department of Earth sciences staffs that helped me whenever necessary. Particular thanks go to Dr. K. S. R. Murthy, Dr. Dereje Ayalew, Dr. Lulseged Ayalew and Dr. Dagnachew Leggesse.

I would like to thank the personnel of National Meteorological Agency and the Woody Biomass for providing me with relevant data and documentations.

I am grateful to the senior Remote Sensing and GIS students: Yodit Teferi and Henok (Kacha) for the materials they give.

My greatest thanks and honor is to GOD. My appreciations also go to my family and fellow postgraduate students for encouraging and support me.

Abstract

The study area, Hosaina-Werabe, is situated in the western margin of the main Ethiopian rift valley. It is structurally controlled and tectonically active. It is covered by loose ash falls, weak pumice layers, and less welded tuff layers, which are vulnerable to land degradation activities, and are intercalated with relatively stronger ignimbrite layers. Whereas the lithologies and geological structures make the area vulnerable to land degradation, the steep slopes at fault escarpments and volcanic domes accelerate the erosive power of overland flows and /or rivers. The main land degradation process is erosion by water.

The land degradation activity in the area is assessed using integrated remote sensing and GIS techniques and field survey. The rate of land degradation, in areal bases, has been estimated using Landsat satellite images of the years 1973, 1984, 2000 G. C. on a small sample site of about 247 sq km. area, which was a subset from the study area. The average rate of land degradation from the year 1984 to 1973 is 0.7 sq. km / year and from the year 1984 to 2000, it is 1.0 sq. km / year. The result shows a general increasing trend of land degradation.

The areal extent of degraded land is also increasing over time. In the year 1973, it was 7.3 %, in the year 1984, it rose to 10.4 % and it was extended to 16.7 % in the year 2000 G. C.

Cross-tabulation of two year images at a time, indicated that few parts of the formerly degraded areas were seen to be covered by vegetation. However, newly formed degraded lands have shown prominent areal expansion through time.

Land degradation vulnerability factor maps were produced from topographic maps, existing maps, Landsat satellite data and SRTM (Shuttle Radar Topographic Mission) data. GIS analyses of distance and area measurements, slope, and reclassification were done for each factor based on their relation with land degradation activity. These layers were standardized and weights were given in a hierarchical order. Finally multi-criteria analysis was done that indicated areas susceptible to land degradation. It was reclassified in order to produce three classes of vulnerability map for the study area. Accordingly, factors that are responsible for making the area vulnerable to land degradation are, in decreasing order of importance: drainage, slope, geological structure, geology (lithology), soil and land use/ land cover.

1. General Introduction

1.1. Introduction

The term land in a broad sense refers to climate, water resources, landforms, soil, and vegetations. Therefore land degradation encompasses soil degradation and the deterioration of natural landscapes and vegetations (Bridges, 2001). Once these materials are lost or degraded, it is extremely difficult, sometimes impossible for them to recover naturally. This is the main reason why land degradation is a serious environmental problem and hence needs important attention.

Principal processes of land degradation include erosion by water and wind, chemical degradation including acidification, salinization, and leaching, while physical degradation includes such processes crusting and compaction. More than half of land degradation events in the world are the results of water erosion (FAO, 1994). A combination of two or more land degradation processes may affect most lands or landscape units.

Land degradation impacts are manifested as a decline in land quality on site where degradation occurs (e.g. erosion) and also off site where sediments are deposited (Eswaran et al., 2001). The impact of land degradation is widespread as it threatens not only the productivity of agriculture but also water quality, biodiversity and the fundamental ecological processes on which life depends (Conacher, 2001).

Land degradation is caused by both human-induced (anthropogenic) and natural factors. Anthropogenic factors include land clearing and deforestation, overgrazing,

intensive farming, poor land management, urbanization, mining activities, road construction activities, population pressure, failure to implement appropriate technologies, poverty, and local agricultural and land use policies (Virmani et al. in Reich et al., 2001), while natural factors include climatic variability, drought, geology (lithology, spatial distribution, contact relationship, texture, structure), topography (slope angle, relief), nature of soils (composition, texture, structure) and vegetation cover (type and density).

Depending on their inherent characteristics and the climate, lands vary from highly resistant or stable to those that are vulnerable and extremely sensitive to degradation. The inherent characteristics of land are its underlying geology and geomorphology, soil type and vegetation cover (Eswaran et al., 2001). Severe losses due to high erosion and deterioration of lands, which are naturally vulnerable to degradation, may be accelerated by the interference of anthropogenic factors.

1.2. Objectives of the study

This study focuses on on-site impacts of land degradation, which is the removal of soil and rock material from the area, and the main land degradation process in the study area is soil and rock material erosion by water. This results in: soil degradation, deterioration of natural landscapes and vegetations, abandonment of cultivated lands, and changes of arable lands into Bad Lands. Such areas have been subsequently abandoned and lead farmers to shift and cultivate other more sensitive areas. This conversion of agricultural lands into Bad Lands has been increasing with time, and it is high time to address this problem scientifically in order to:

1. Show the significance of the underlying geology in determining the vulnerability of the land to degradation;
2. Calculate the rate and the extent of the degradation in the area, in areal bases, using GIS-RS techniques;
3. Identify and delineate the most affected areas and correlate them with specific natural and man-made factors;
4. Make the local people and local government aware of the existing problem by providing research results;
5. Recommend possible prevention methods against the problem.

Therefore, the general objectives of the research were to

- study the underlying geological factors affecting the vulnerability of land to triggering factors of degradation such as water erosion;
- delineate vulnerable areas by producing susceptibility maps of land degradation for land use management purposes.

And the specific objectives of the work were to

- asses the areal extent of land degradation in the study area using remote sensing and GIS techniques;
- investigate temporal changes in the extent of land degradation and asses the rate of land degradation using remote sensing and GIS techniques;

1.3. The Study area

1.3.1. Introduction

This study evaluates the underlying geological setup in relation to the vulnerability of land to degradation. In the study area, land degradation activity is manifested not only by soil erosion but also by the deterioration of natural landscape and vegetation. It is observed that land degradation activity affects not only the soil cover but in many places also involves removal of the bedrock. There is both soil degradation and the deterioration of natural landscapes and vegetations, as a result of the removal of both soil and rock materials that result in the formation of gullys, inselbergs and badlands (Plates 1 and 2). The observed land degradation might have started either as sheet or rill or gully erosion by rainwater runoff or / and river.

Plate 1. Land degradation features in the study area.

Plate 2. Different erosion features, those manifesting the existence of intense land degradation in the study area.

This study focuses on the relationships between land degradation activity and the underlying geology. Land can be naturally vulnerable due to its underlying geology that determines the inherent weakness of the rock attributed to its lithology, distribution of various lithologic units, presence of geological structures and geomorphologic settings.

A naturally vulnerable land can be easily affected by triggering factors. The main triggering natural factor for land degradation in the study area is water erosion. In most places of the study area, removal of soil and rock started as sheet and rill erosion and expanded to gullys and isolated inselbergs, and finally developed to Bad Lands.

Delineation of the study area was done by direct observation of intense land degradation problem in the area. It is assumed that the occurrence of intense land degradation in the study area is mainly related to the underlying geology that is lithology, and geological structures.

1.3.2. Location, areal extent and accessibility of the study area

The study area is located in the south central part of Ethiopia along the main Addis Ababa-Hosaina road, in between the towns of Werabe (about 174 Km from Addis Ababa) to the Northeast and Hosaina (about 232 Km from Addis Ababa) to the Southwest. It is located in zone 37 UTM grids of 870031 meter N to 832792 meter N, and 393096 meter E to 424110 meter E and 364415 meter E to 397272 meter E. It covers an area of about 1199 square Kilometers.

The area forms part of three administrative zones: Hadiya zone, Gurage (currently reclassified as Silti) zone and Kembata-Alaba-Tembaro zone.

The area is easily accessed along the main Addis Ababa-Hosaina asphalt road (currently under major maintenance) and along gravel roads that connect rural towns and markets to the main road (Fig. 1).

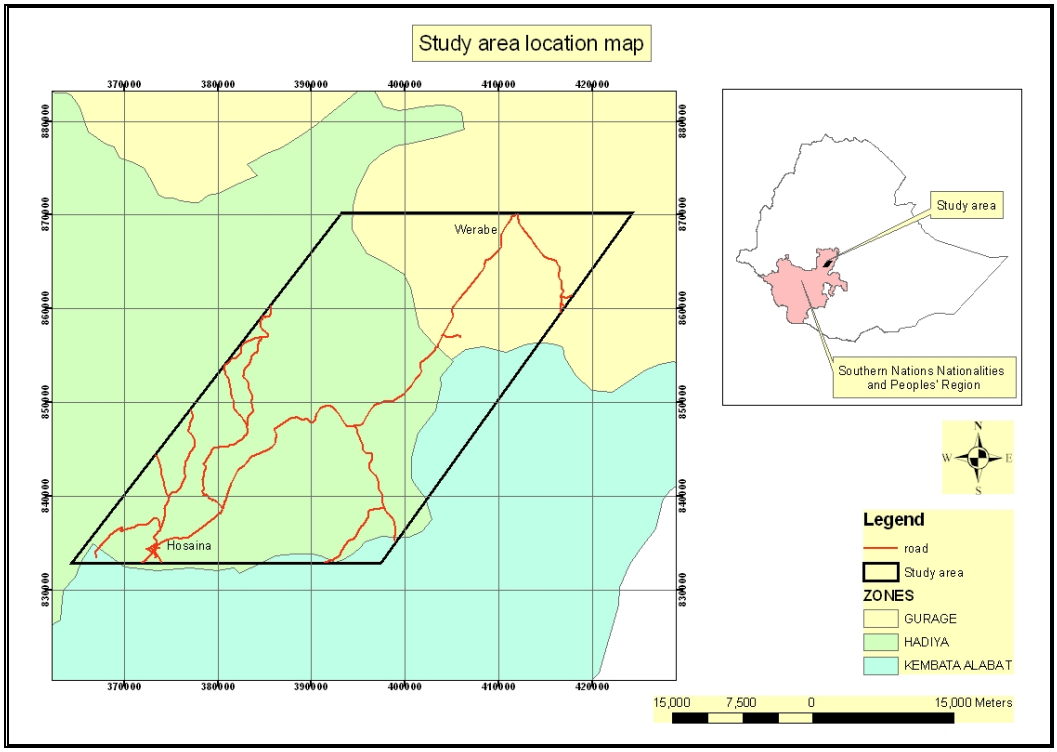

Figure 1. Location map of the study area (study boundary and road data layer is digitized from the topographic map of 1978 G. C. and zone data layer is from Ethio-GIS data).

1.3.3. Topography and landforms

The area is located at the western margin of the main Ethiopian rift system and it is structurally controlled, and tectonically active. Normal fault escarpments and volcanic domes form most of the elevated ridges and landforms (Figs. 2 and 3). The topographic elevation of the study area ranges from 2920 meter above sea level on the upper left side to 1880 meter above sea level at the right edge (Fig. 2).

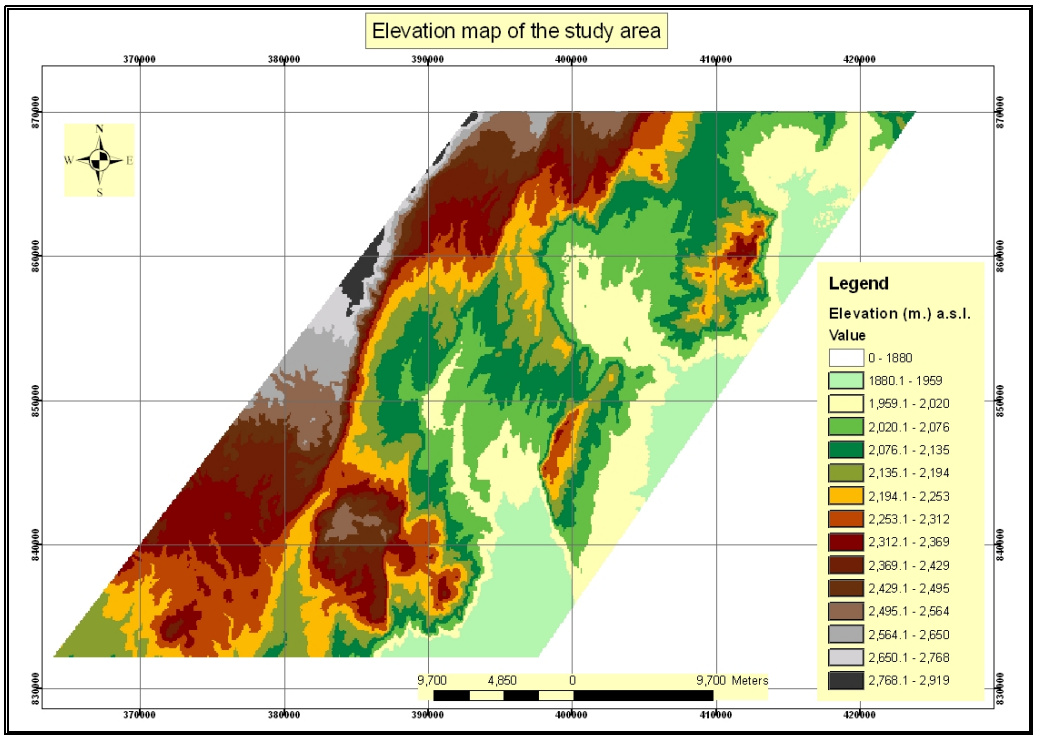

Figure 2. Elevation map of the study area (based on SRTM data of 2000 G. C.).

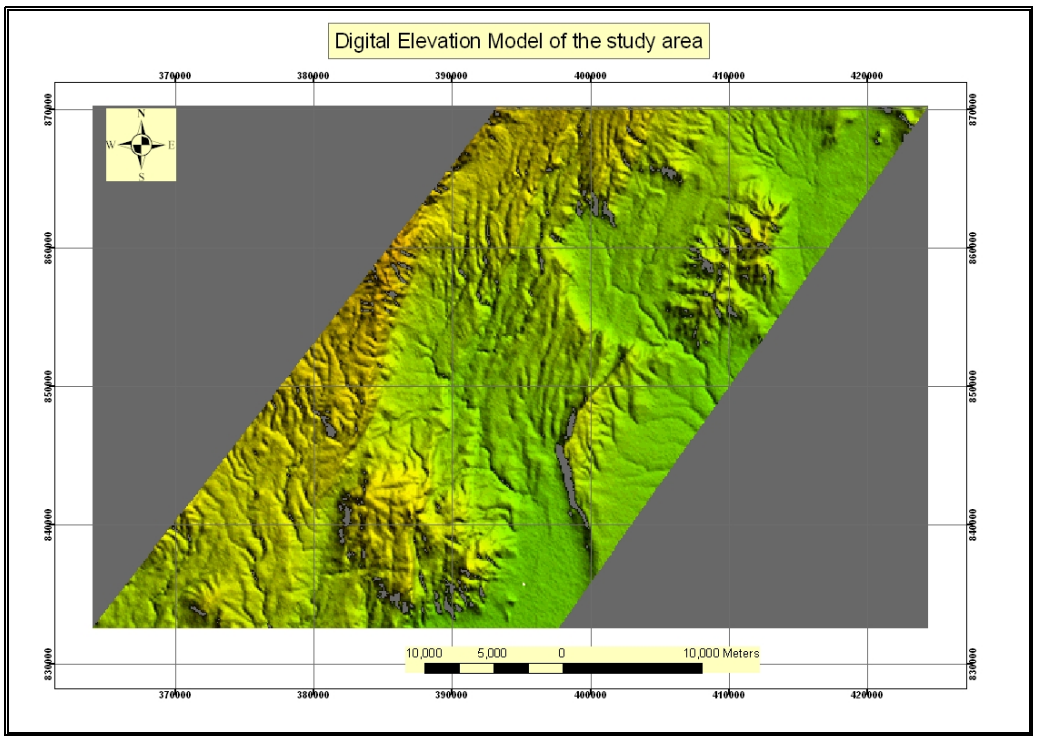

Figure 3. Digital Elevation Model of the study area (from SRTM data of 2000 G. C.).

1.3.4. Soil

According to Ethio-GIS, there are ten soil types in the study area (Fig. 4): calcic xerosols, chromic luvisols, chromic vertisols, eutric cambisols, eutric fluvisols, eutric nitisols, leptosols, orthic solonchakes, pellic vertisols, and vitric andosols, based on the FAO/UNESCO system of soil classification.

The major soil types on the area are orthic Solonchaks, chromic Vertisols, vitric Andosols and eutric Fulvisols: Solonchaks are salty soils with little horizon development, Vertisols are dark colored, cracking and swelling clays when they are dry, Andosols are dark soils formed from volcanic materials with little horizon development and Fulvisols are alluvial an flood plain soils (Office of Arid Lands Studies, 2001).

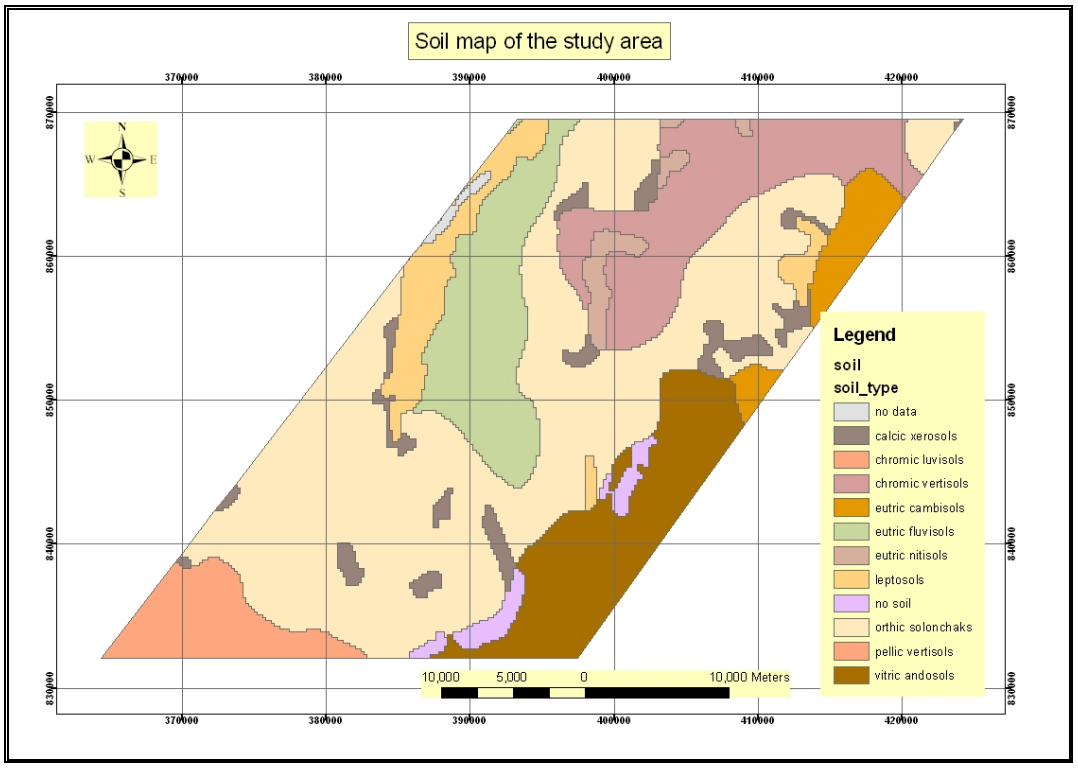

Figure 4. Soil map of the study area (from Ethio-GIS).

1.3.5. Drainage

Drainage map of the area, digitized from the topographic map, indicates that the drainage system is strongly influenced by the underlying geological structures (Fig. 5). Dendritic drainage patterns are common in almost all areas. The major streams form parallel drainage pattern oriented in a general North-South direction, following the direction of major structural lines. The tributaries form dendritic drainage pattern while some radial drainage patterns are observed along slopes of volcanic domes.

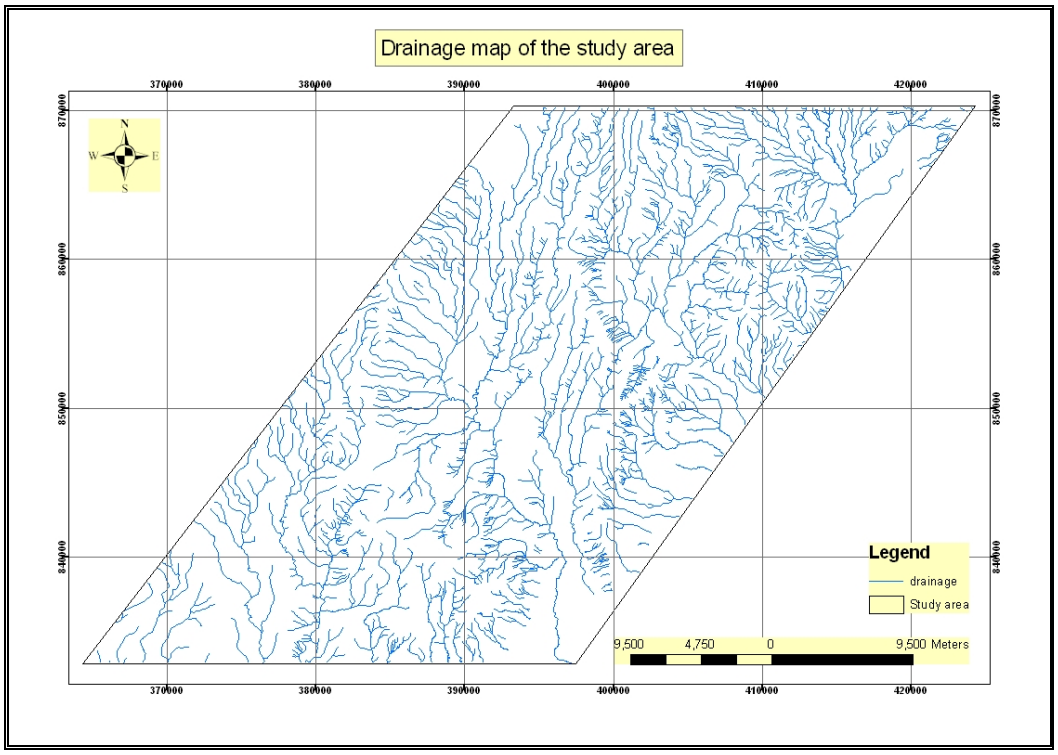

Figure 5. Drainage map of the study area (digitized from the mosaic topographic map).

1.3.6. Land use / land cover

Land use / land cover map of the study area is modified from Woody Biomass Land use/land cover base map of Ethiopia (Woody Biomass, 2001). The map is clipped in ArcGIS using the study area boundary map (Fig. 6). Additional features including open forests, water body, degraded areas and wetlands were digitized from Landsat 7 image of the year 2000 G. C. of the same area. Identification and interpretation of the latest available satellite image was made using various colour composites, such as the common false color composites of 432 in RGB (red, green and blue) order, was supported by point GPS data and results of actual field survey in the area.

According to the Woody Biomass (2001) report, the administrative zones of Gurage, Hadiya and Kembata-Alaba-Tembaro have a high percentage of area under cultivation. Enset is the dominant main element of a diet hence enset with cereals are the main land use systems. Enset is found in the highlands between 1,600 and 3,000 m a. s. l.; coffee below 2,000 m a. s. l.; chat, sweet potato, fruit trees and cabbage are grown in the household garden, or an enclosed infield next to the homestead. In unenclosed outfields, cereals are cultivated: maze, tef and sorghum are found below 2600 m a. s. l. and wheat and barley above 2600 m a. s. l.

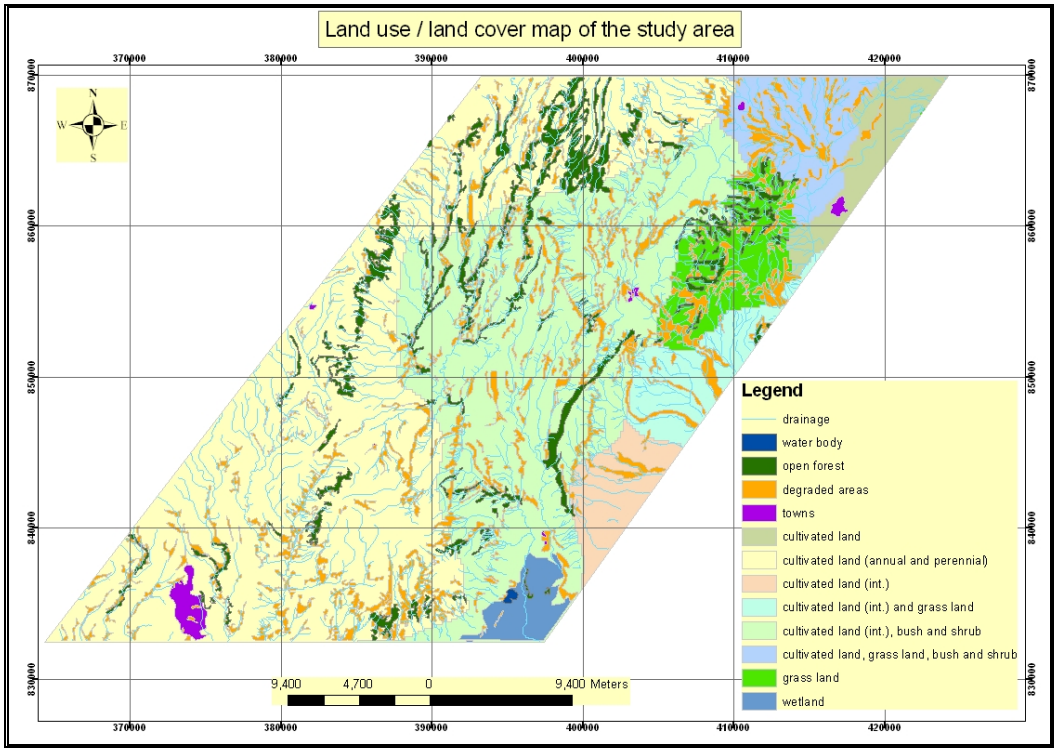

Figure 6. Land use/ land cover map (modified from Woody Biomass, 2001).

1.3.7. Rainfall and Temperature

Monthly rainfall and monthly minimum and maximum temperature data of available years (from year 1953 G. C. to 2005 G. C.) has been used from Hosaina Meteorological station for this study. However, there are gaps in the data set (monthly rain fall data are missing for years 1969-1971, and 1984 G.C.; temperature data are missing for years 1969-1971; 1984; 1986; 1987; 1993, and 1994 G.C.).

Generally there are three distinct seasons in the area with respect to rainfall distribution (Fig. 7a): (i) the short rainy season from March to May (belg); (ii) the heavy rains from June to September (kiremt); and (iii) the long dry period (with little or no rain) from October to February (bega).

The minimum and maximum temperatures data shows very small variation (Fig. 7b). Minimum temperature shows general increasing tendency. The maximum temperature shows constant tendency except from year 1954 to 1959 G.C. that had higher values.

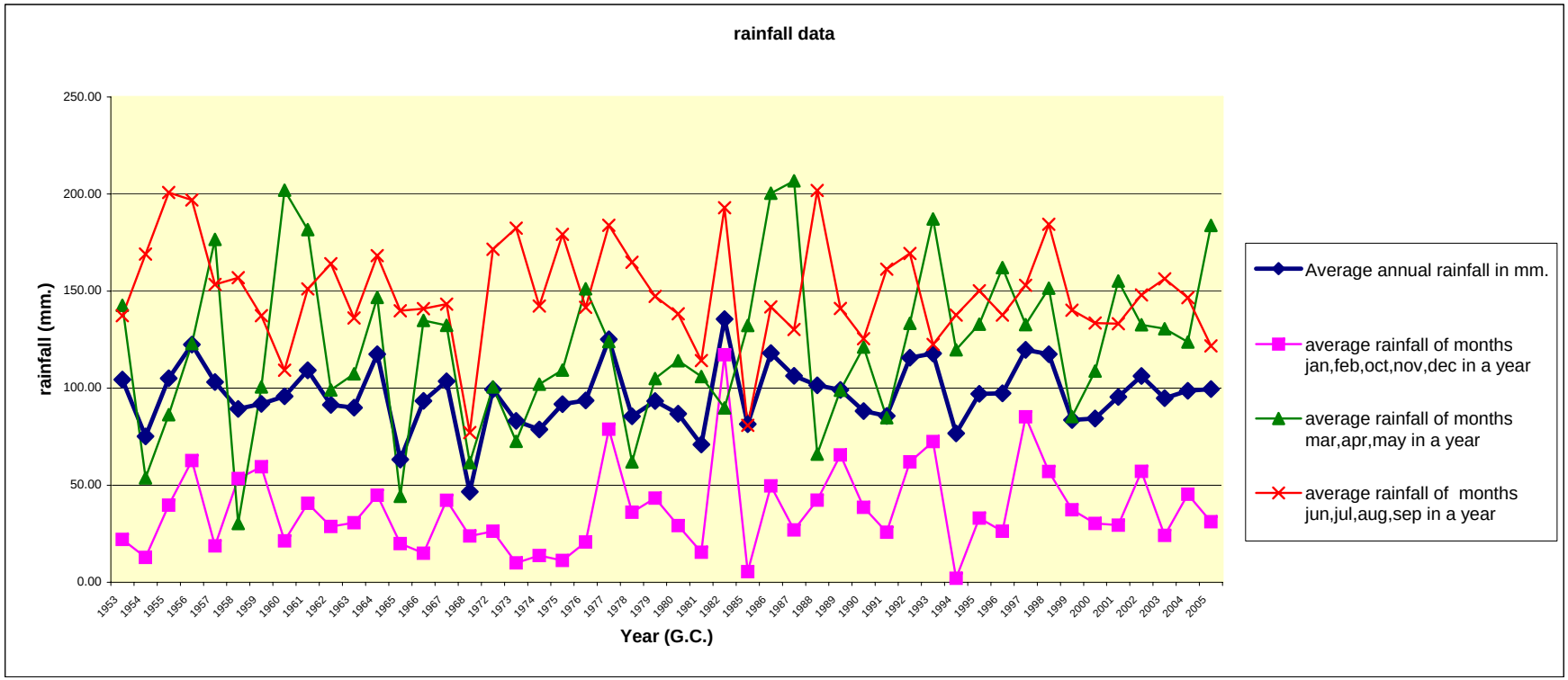

Figure 7 (a). Rainfall in millimeters (**1. blue**: average annual rainfall; **2. pink**: average rainfall of the months January, February, October, November, and December in a year; **3. green**: average rainfall of the months March, April, and May in a year and **4. red**: average rainfall of the months June, July, and September in a year).

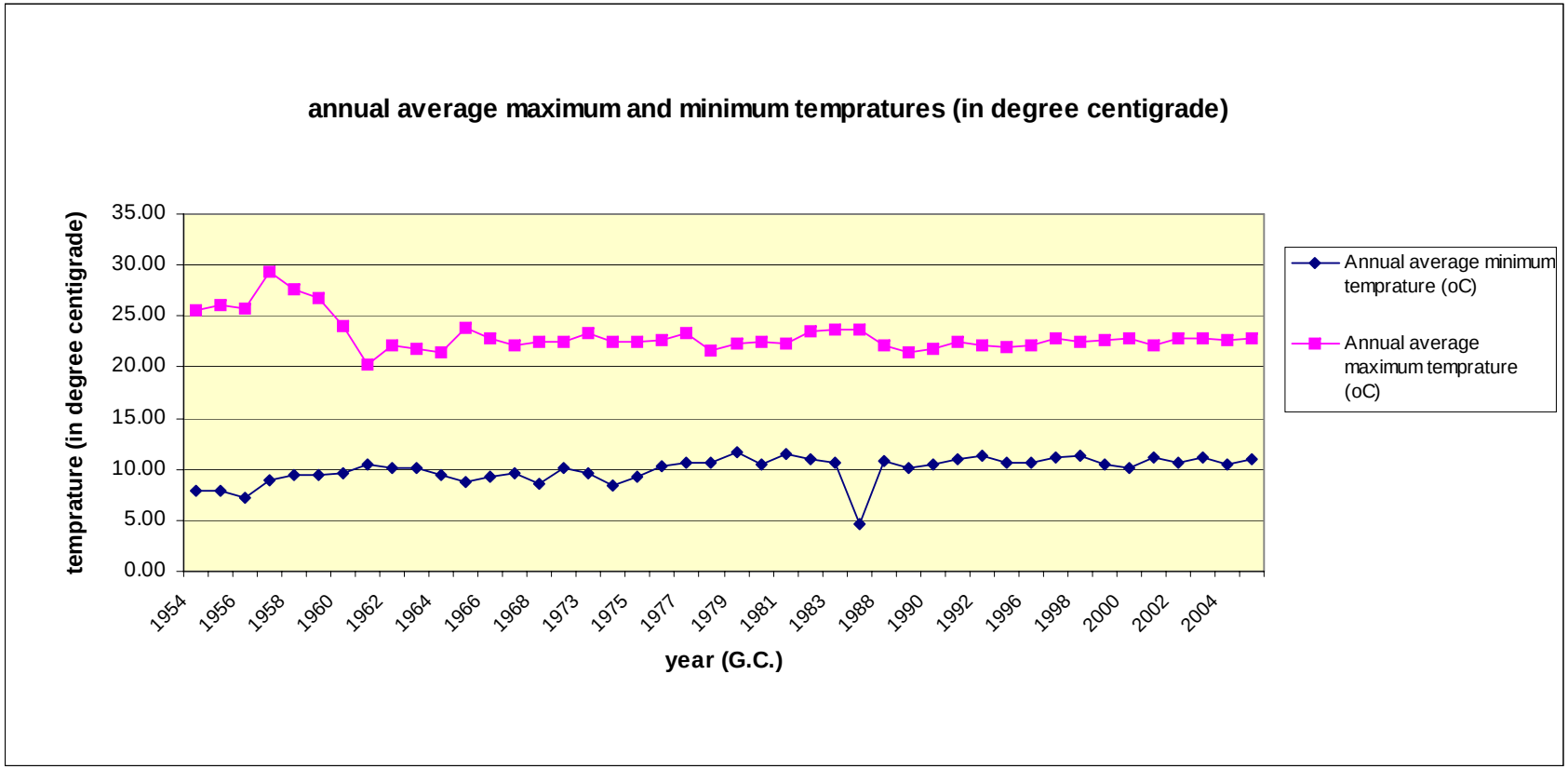

Figure 7 (b). Annual average maximum and minimum temperatures (in degree centigrade).

1.3.8. Population

In Ethiopia population and housing census was conducted two times, the first in May 1984 G. C. and the second in October 1994 G. C. In the 1994 census, the total population of Southern Nations, Nationalities and Peoples' Region was found to be 10,377,028 of which 704,818 were urban and 9,672,210 were rural. Population projection was done for each year from 1995 to 2000, based on the assumption that the national annual average population growth rate of rural and urban areas for the observed from 1984 to 1994, which were 2.23 percent and 4.11 percent respectively, will remained constant during the projection periods. The projection is made for a limited number of years and under very broad assumptions. Therefore, at the year 2000 the total population of the region would be 11,879,455 of which 891,498 are urban and 10,987,957 are rural (CSA, 1996).

In the 1994 census, the population of the Gurage Zone was 1,556,964 of which 76,988 were urban and 1,479,976 were rural, that of the Hadiya Zone was 1,050,151 of which 67,705 were urban and 982,446 were rural, and for the Kembata-Alaba-Tembaro Zone it was 727,340 of which 50,987 were urban and 676,353 were rural.

The data shows that the rural population is significantly higher than the urban and the main livelihood of the rural population is agriculture. Over decades there has been a shift from an agro-pastoral system towards mainly agricultural due to progressive shortage of grazing land and therefore now there is a decline in livestock asset per household (Woody Biomass, 2001).

2. Land degradation problem

2.1. Land degradation

Land degradation will remain an important global issue for the 21st century because of its wide impact on agronomic productivity, the environment, and its effect on food security and the quality of life (Eswaran et al., 2001). Ethiopia is a developing country and more than 80% of its population depends on agriculture for its subsistence. This situation lead to mainly agrarian economy which, under most conditions, is under the mercy of natural and man-made environmental problems including land degradation.

Land degradation is a slow and hardly noticeable process of which many people or farmers are not aware of their land is degrading.

According to UNEP (1999), land degradation has affected some 1900 million hectares of land worldwide. The loss of potential productivity due to soil erosion worldwide is estimated to be equivalent to some 20 million tons of grain per year. The rate at which arable land is being lost is increasing and it is currently 30-35 times the historical rate. In Africa an estimated 500 million hectares of land have been affected by soil degradation, including 65% of the region's agricultural land.

Land degradation activity on a certain area is a function of all environmental components, which are inter-related to each other. These factors or components are different from place to place. Each component has its own response to land

degradation activity, and also they are interacting with each other during the land degradation process.

2.2. Forms of land degradation

The main forms of land degradation are erosion by wind and water. Water erosion covers all forms of soil erosion by water, including sheet, rill and gully erosion. Water erosion depends on the intensity of precipitation and runoff, the slope of the terrain (where on high slopes river erosivity works with mass movement), nature of the soil and the underlying rock units, absence or presence of vegetation cover. On bare fields, the rate of soil erosion by water is very high (Warren et al., 1988).

Water erosion process consists of discrete stages from raindrop impact to the formation of gully erosion and each stage has its own processes and characteristics. Controlling or preventing water erosion (land management) requires an understanding of each step in the erosion process. The steps are splash, sheet, rill and gully erosion.

Splash erosion (rain drop impact): Loose friable surface with no protective vegetation cover (no trees to break the direct fall of rain) results in splash erosion. Splash erosion results in the formation of surface crusts, which reduce infiltration and enhance runoff, which initiates sheet and rill erosion.

Sheet erosion: occurs as a shallow sheet of water flowing over the ground surface resulting in the removal of a uniform layer of soil from the soil surface.

Rill erosion: results from the concentration of surface water (sheet erosion) into deeper, faster flowing channels.

Gully erosion: is an advanced stage of rill erosion. Gully erosion is responsible for removing vast amounts of soil, destruction of farmland, roads and other engineering structures.

2.3. Previous Works

Land degradation problem has been addressed by a number of researchers. Land degradation is one of the consequences of mismanagement of land and results frequently from a mismatch between land quality and land use (Beinroth et al., 1994, in Reich et al., 2001).

Most of works indicated that human induced land degradation is a critical problem in sub Saharan Africa including Ethiopia. This is attributed to increasing population pressure leading to cultivating marginal lands already susceptible or vulnerable to various forms of degradation (FAO, AGL, 2000), poverty and lack of agricultural intensification (lack of mechanized farming activities) (Nyssen et al., 2004) or soil erosion and deteriorations of soil structure due to heavy grazing (Tekle, 1999). Drainage practices on farm fields, inappropriate land use system and inappropriate land tenure policies aggravate land degradation processes in Ethiopia (Taddesse, 2001).

Although the manifestations as well as the consequences of human-induced (anthropogenic) land degradation have been well studied, very few works focused on the natural vulnerability of land to degradation due to geological and geomorphological factors. Some works (e.g. Stahl, 1990; Girma and Jacob, 1988; in Nyssen et al., 2004) hinted that erosion processes on the Ethiopian highlands are caused by the combination of erosive rain and steep slopes due to the quick tectonic uplift during Pliocene and Pleistocene.

In the central part of the Ethiopian rift system, the very recent and still active tectonic deformations and volcanism produce dynamic features with steep hilled volcanoes, rough lava fields and wide areas covered by ash and pumice making them vulnerable to erosion. Moreover rift margin escarpments with neo-tectonic features as well as the lowering of base levels due to lake level falls have been reactivating erosional processes. Consequently in this naturally fragile area, any climatic and anthropogenic modification can give rise to degradation of natural resources (Sagri, 1998).

Land degradation is a common environmental problem in Ethiopia, but basic understanding of the underlying causes governing vulnerability of land to degradation has been less emphasized. It is assumed that the existence and rate of land degradation depends on the background flexibility to triggering factors: lithology, geological structures, geomorphology, slope and drainage patterns, weathering and soil characteristics are the major background factors that may aggravate the effect of triggering factors or increase the resistance against land degradation.

3. GEOLOGY

3.1. Regional geology

The study area is located in the western central part of the main Ethiopian rift valley. The main Ethiopian rift is characterized by active extensional tectonics and it is seismically, tectonically and volcanically active (WoldeGabriel et al., 1990). Volcanic rocks of Pliocene and Pleistocene age such as rhyolites, trachytes, and ignimbrites are abundant within the rift floor and on the adjoining plateaus (Kazmin, 1975 in Mahatsente et al., 1999).

In the rift, a number of major centers of silicic volcanism occurred in relation to the zone of intense faulting (Mahatsente et al., 1999). The main trend of tectonic structures in the main Ethiopian rift is dominantly NNE-SSW direction (Mohr, 1962b in Mahatsente et al., 1999) and in some places NE-SW direction (Meyer et al., 1975 in Mahatsente et al., 1999).

According to woldeGabriel et al. (1990) the geochronological sequence of the western escarpment of the Main Ethiopian Rift valley at Gurage is represented by the following stratigraphic units:

The crystalline basement: is represented by altered biotite gneiss intruded by groups of northwest trending quartzofeldspathic pegmatites. This basement around Guraghe was not dated but radiometric dates on crystalline basement elsewhere in Ethiopia ranges from 1.1Ga – 470 Ma (Asrat et al., 2001).

The Mesozoic sequence: is widely found in Ethiopia and unconformably overlies the crystalline basement in Guraghe. The Mesozoic sequence is much thinner here: 150 m. of Early Jurassic Adigrat Sandstone, 20 m. of variegated shale, and 30 m. of Jurassic Antalo Limestone (Arno et al., 1981 in WoldeGabriel et al., 1990). The cretaceous strata present elsewhere in the platform Mesozoic sequence of Ethiopia, is absent.

The pre-Tertiary Oligocene basaltic flows and fluvial strata: Fine-grained Oligocene basaltic flows (32 Ma.) having 40 to 60 m. thickness are overlain by fluvial strata of 2 to 10 m.

Pliocene basalt flows, crystal rich welded tuff and ash fall tuffs: The pre-tertiary rocks, the Oligocene basalt, and the fluvial strata are unconformably overlain by a thick sequence of Pliocene basaltic flows of 4.2-2.5 Ma. age and by a crystal rich welded tuff having a thickness of 200-250 m. and age of 3.2 Ma. A number of Late Pliocene ash fall tuffs having an age between 3.72 and 2.59 Ma. cover the sequence.

According to WoldeGabriel et al. (1990), the sequence of volcano-tectonic events that formed the western rift margin at Guaghe, from old to young are:

1. Block faulting and tilting of pre-Tertiary rocks and mid-Oligocene basaltic eruptions
2. Sedimentation and faulting
3. Eruption of thick, late Miocene, flood basalt

4. Late Miocene faulting, eruption of an 8.3 Ma. Ignimbrite and Pliocene flood basalt and ignimbrite formation and
5. Plio-Pleistocene faulting

3.2. Geology of the study area

In the study area, three lithologic units out crop: the ignimbrite and tuff unit, the rhyolite unit occupying higher areas and the pyroclastic and volcanoclastic sedimentary unit in low lands (Fig. 8). The ignimbrite, tuff and rhyolite rocks are referred to as the Butajira Ignimbrite (WoldeGabriel et al. 1990). According to WoldeGabriel et al. (1990) the Butajira Ignimbrite unit dates back to early to middle Pliocene (3 - 4.2 Ma.), an epoch characterized by the eruption of voluminous silicic pyroclastic material (from the Awasa caldera, the Wagebeta caldera complex and major caldera probably buried beneath the Ziway-Langano-Abiata basin) and by subordinate basalt flows.

In the study area, the Ignimbrite and tuff unit contains alternating layers of Ignimbrite, tuff, pumice and ash fall of varying texture, strength, and degree of weathering. The rhyolite domes contain associated obsidian flows.

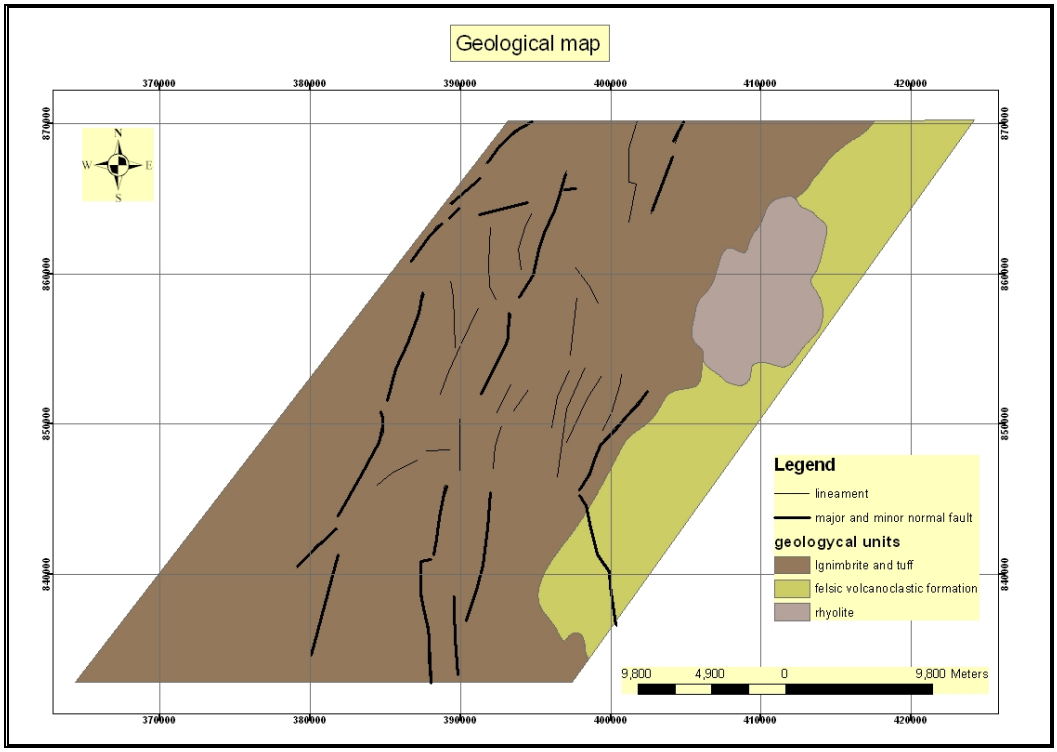

Figure 8. Geological map of the study area (Modified after Tadesse et al., 2004).

3.2.1. Lithostratigraphy

Field survey along some selected traverses in parts of the study area, where intensively affected by land degradation (Fig. 9), revealed the following units:

Ignimbrite and tuff

The ignimbrite unit is made up of alternating sequences of four sub-units of different textures leading to differential strength along the succession, which, in turn, resulted in differential erosion (Plates 3, 4 & 5). These units are:

- The ignimbrite layer: this is relatively strongly welded. This layer is relatively slightly weathered to fresh, and at some places it is moderately to highly weathered. It forms vertical walls where it layover weak layers.

- The tuff layer: this is less welded, coarse grained (lapilli size) and it is weak to very weak (Plate 3).

- The ash layer: this is loose to moderately compact, and very weak (Plate 4).

- The pumice layer: this is relatively compact and moderately strong (Plate 6).

3.2.2. Geological structures

The rift floor ignimbrite unit is affected by generally North–South oriented vertical fracture systems. Major drainage systems are focused along the fracture lines, in turn, focusing erosion features along them. Erosion and transportation of materials along these fractures initiate rills and/or gullies (Plate 6), which may lead to the formation of inselbergs (isolated hills and mountains) and Bad Lands. This process is facilitated by the weakness and less resistant nature of the underlying geological materials. Slopes formed along fault escarpments are easily affected by erosion and degradation processes.

For the study area, geological structure mapping has been done using Landsat ETM+ panchromatic image of the year 2000. Directional filter is done at 0^0 and 20^0 in order to enhance and visualize the lineaments easily. This map is verified using the DEM of the area and structural measurements during field survey.

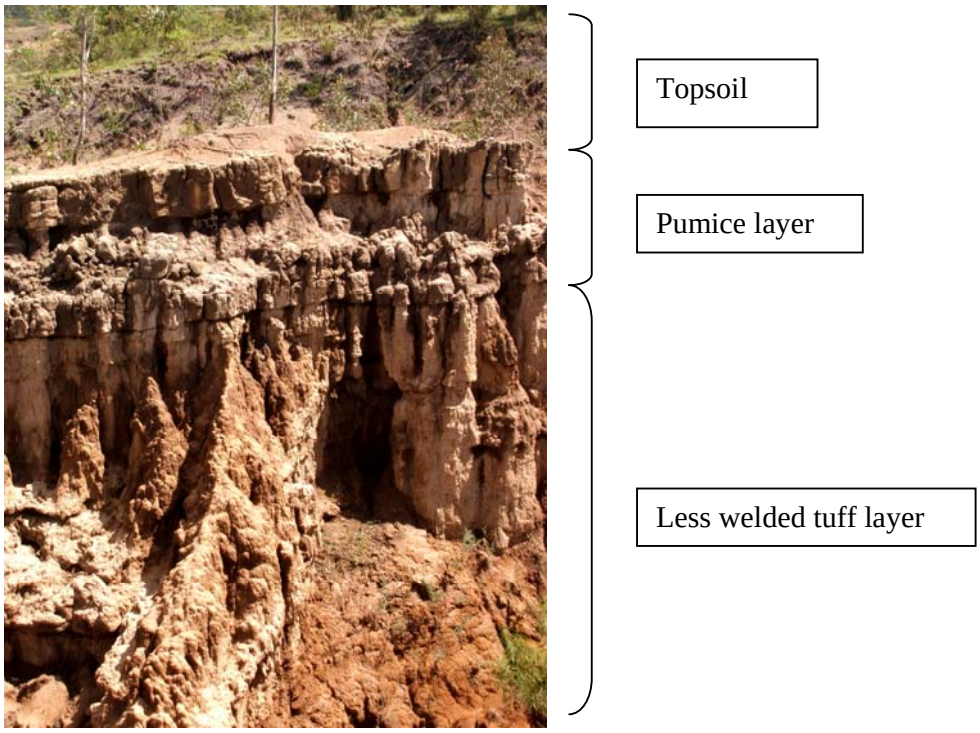

Plate 3. Different layers exposed by land degradation.

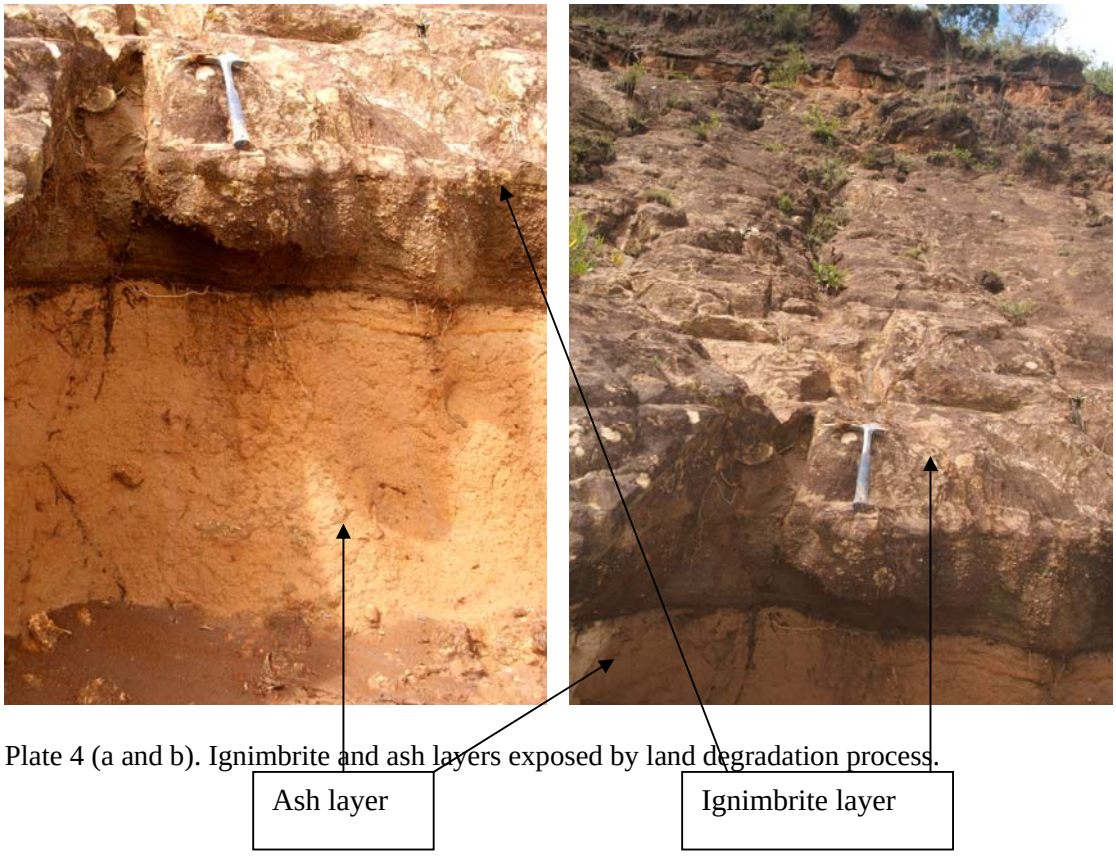

Plate 4 (a and b). Ignimbrite and ash layers exposed by land degradation process.

. Plate 5. Pumice layer.

Plate 6. Drainage focus and follows geological structure and initiate rills or gullys on the Ignimbrite, which finally leads to the formation of inselbergs or badlands.

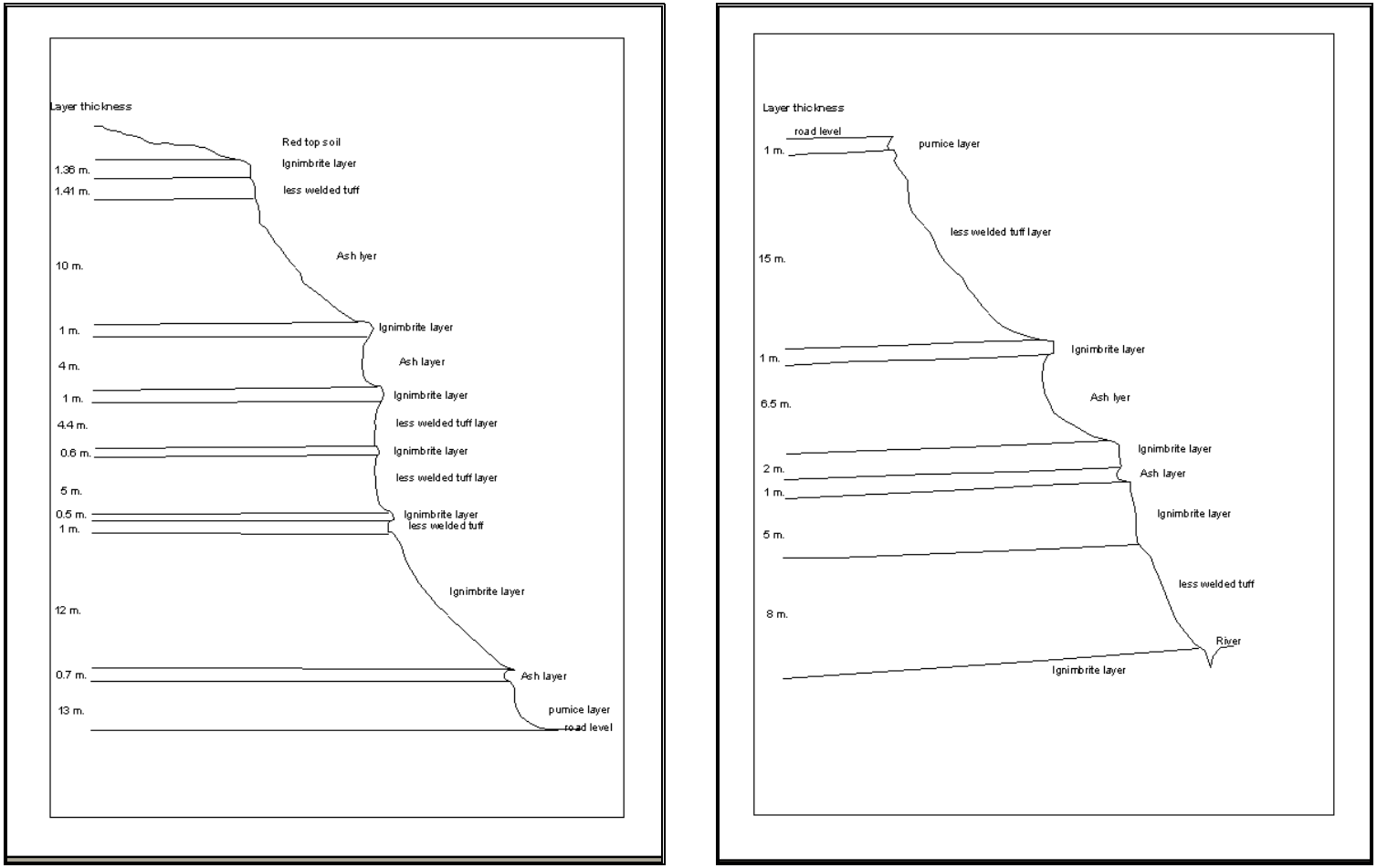

Figure 9. Lithostratigraphy of the rift floor ignimbrite from two traverses during field survey.

4. REMOTE SENSING AND GIS TECHNIQUES

4.1. Introduction

Satellite images can be used as a spatial reference of areas and as a base for information derivation through data processing and analysis. Satellite image can aid the physical acquisition of field data by providing a means, for example, for choice of sample area in favor of evaluation of the rate and spatial variation of land degradation from the study area, and for mapping and identifying features using different RGB color composition to be verified (or matched) in the field. The joint interpretation of satellite images and field data can greatly aid the extraction and evaluation of information. Field data reduce the workload associated with visual satellite image interpretation. Use of previous maps, for the task of interpretation of current land use / land cover and lithology, also facilitates the work.

Data transformation, in digital image processing, generally refers to a mathematical operation on satellite image spectral data for enhancing the interpretation or for discriminating the selected terrain features. It reduces the data volume and the influence of scene-to-scene brightness variations due to sun angle. The output of all data transformation is amenable to interpretation and all forms of digital analysis, including digital classification. Unsupervised and supervised classification changes the total scene into a limited number of major classes and gives a general idea of the area.

A final step in the image interpretation process may involve digitizing the results. Digitizing enables capturing the information in computerized special database format for subsequent individual and joint analysis with other spatially formatted data in GIS.

Materials used

The following materials have been employed in this study for the assessment of land degradation process, mapping and evaluation using remote sensing and Geographical Information System (GIS) integrated with field survey:

1. Five topographic maps of year 1978 G. C., having a scale of 1:50,000 (Table 1): were used during field survey, digitization of road network, drainage network, contour, towns and market places.

Table 1. Topographic sheets that were used for this study.

Index to adjoining topographic sheets	
GEJA	0737B2
HOSAINA	0737B4
DALOCHA	0738A1
WILBAREG	0738A3
TORA	0738A2

2. Landsat 1 satellite MSS data of the year 1973 G. C. with four bands is used for detailed mapping of the degraded area on the sample site for a time series analysis.
3. Landsat 5 satellite TM data of the year 1984 G. C. having seven bands was also used for time series analysis of the extent and rate of land degradation.

4. Landsat 7 satellite ETM+ data of the year 2000 G. C. having eight bands was mostly used (it is the only latest available data for the area).
5. SRTM (Shuttle Radar Topographic Mission) data of the year 2000 G. C. was used to produce elevation map.
6. GPS, compass, digital camera, geological hammer, measuring tape and hard copies of different color compositions of satellite images were used during field survey.
7. Land use / land cover map of Ethiopia from the Woody Biomass (2001) with a scale of 1:2,000,000 was used as a base map for detailed land use / land cover mapping of the area.
8. The Geology and mineral map of Ethiopia at a scale of 1:2,000,000 (Tadesse et al., 2004) and maps from WoldeGabriel et al. (1990) were used as bases to produce the geological map of the study area.
9. The Ethio- GIS data was used to produce zone boundary and soil type of the study area.

Softwares used

1. ERDAS Imagine 8.6: used for georeferencing, digitization and image analyses.
2. ENVI 3.5 and ENVI 4: used for visual interpretation and image analyses.
3. ArcView GIS 3.2a and ArcGIS 9: used for GIS analysis and mapping.
4. IDRISI 32 release 2: used for GIS analysis.
5. Global mapper: used to extract elevation data.

4.2. Remote sensing analyses

The study area is delineated using five topographic maps of scale 1:50,000, which are scanned by A4 size canon scanner. It produced 18 pieces of A4 size topographic sheets. These pieces were imported to ERDAS IMAGINE 8.6 software and each piece has been georeferenced based on the topographic map projection: UTM zone 37, spheroid Clark 1880 (modified) and datum Adindan. Then it is again re-projected to UTM zone 37, spheroid and datum WGS 84 in order to work with images that have this map projection. Following re-projection of the 18 pieces of topographic sheets, an AOI layer was generated from each piece, then sub-set the AOI layers, and subsequently a mosaic was prepared from the sub-set pieces (Fig. 10). Delineation and sub-setting of the study area, on screen digitization of terrain features (including main road, towns and markets, drainage networks and contour lines) were done on the mosaic topographic sheet.

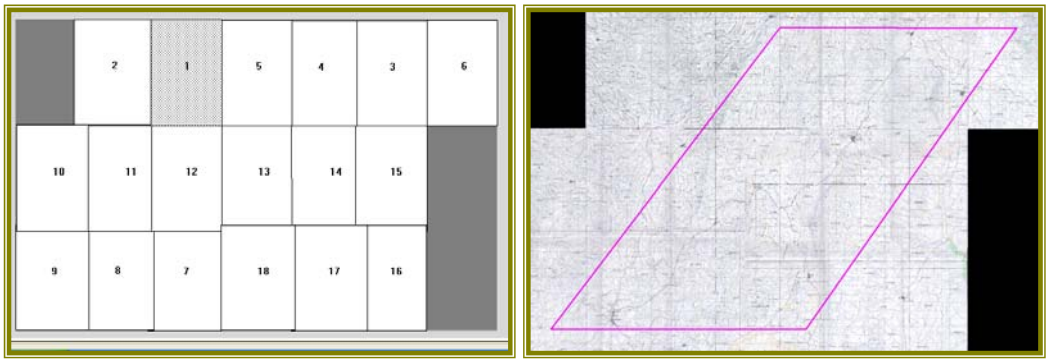

Figure 10. Scanned 18 pieces of topographic map (left), and final mosaic topographic map (right).

Satellite image of Landsat 7 sensor ETM+, path 169 and row 55, which was acquired on January 27, 2000 and processed Sep 09, 2001 (with a map projection of UTM zone 37, spheroid and datum WGS 84) has been used for most of the processing and mapping activities since it is the recent available image. From this image, 7 bands were used: Bands 1, 2, 3, 4, 5 and 7 in visible, near infrared and far infrared electromagnetic spectrum having spatial resolution of 25 meters and band 8 is panchromatic having 12.5 meter spatial resolution (Fig. 11). This image was imported to ERDAS IMAGINE 8.6 software and the study area was subset from the full scene of path 169 and row 55. On the subset image of band 8, directional filter was done in order to digitize the existing geological structures. Printouts of different band combinations were used to identify features during field survey. General land degradation mapping was done on the subset of this image with false color composition of bands 743 in RGB (red, green and Blue) order. This composition enhances soil and rocks and gives light pink (violet) color.

For detailed land degradation mapping and analysis, a sample area of about 247 km sq. was selected from the study area, based on intense land degradation observed during field survey and on color composition of bands 743 of the year 2000 G. C. image. In order to conduct time series analysis, images of the year 1973 and 1984 G. C. were additionally used.

Landsat satellite image of the year 1973 G. C., sensor MSS, path 181 and row 55, which were acquired on January 31, having map projection UTM zone 37, spheroid and datum Clark 1866 was re-projected to UTM zone 37, spheroid and datum WGS 84 using ENVI software, in order to synchronize it with other maps and images. This

image has four bands with a spatial resolution of 57m. This, being the early satellite, digital MSS data were supplied in computer compatible tape (CCP) format, the image was re-sampled into pixels having a nominal dimension of 57 by 57 meter (Lillesand, 2000). This image was used only for detailed land degradation mapping using 465 band combinations in RGB order.

Landsat image of the year 1984 G. C., sensor TM, path 169 and row 55, acquired on November 22, with map projection of UTM zone 37, spheroid and datum WGS 84. It has seven bands with a spatial resolution of 28.5 meter except band 6, of which only three bands are used for land degradation analysis. This image was also used for detail mapping and time series analysis of land degradation, using 743 band combinations in RGB order.

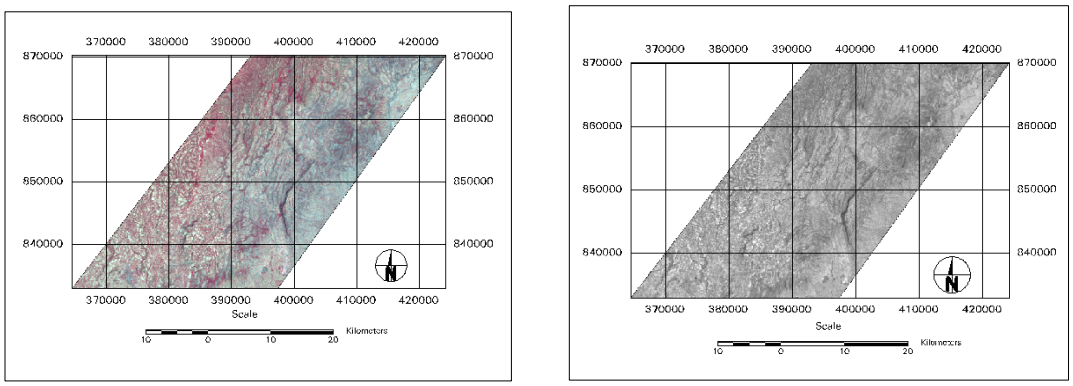

Figure 11. Study area images of year 2000 G. C., false color composite of bands 432 in RGB (left) and panchromatic Band 8 (right).

The SRTM data is exported as digital elevation model (DEM) using Global mapper software form which elevation and slope data layer were produced. The Shuttle Radar Topographic Mission (SRTM) produced digital topographic data for all land areas between 60^0 north and 56^0 south latitude with data points located every 3 arc second

(approximately 90m.) on a latitude/ longitude grid (Ramirez, 2006). This SRTM data is verified by elevation contour data digitized from the mosaic topographic map.

Digital image processing

To extract meaningful information from the imagery and to use remote sensing data, we must perform image interpretation and analysis. Interpretation and analysis of remote sensing data involves identification and / or measurements of various features in the imagery in order to extract useful information about them.

Most common image processing function can be categorized into four.

Pre-processing

Pre-processing is done before the main data analysis and extraction of information. Pre-processing involves two major processes: geometric correction and radiometric correction or haze correction.

Remote sensing imageries are inherently subjected to geometric distortions. These distortions may be due to the perspective of the sensor optics, the motion of the scanning system, the motion of the platform (the platform altitude, attitude and velocity), the terrain relief, or the curvature and rotation of the earth (Lillesand, 2000). Geometric corrections are done in order to compensate for these distortions so that the geometric representation of the imagery will be as close as possible to the real world. Many of these variations are systematic or predictable in nature and accurate

modeling of the sensor and platform motion and the geometric relationship of the platform with the earth correct these distortions.

Other unsystematic or random distortions cannot be modeled and corrected. Therefore, geometric registration of the image to a known ground coordinate system must be performed using ground control points, and corrected images (image to image registration). The Landsat satellite data, used in this study, are all systematically corrected.

Image enhancement

Image enhancement is used to increase the details of the image by assigning the image maximum and minimum brightness values to maximum and minimum display values, and it is done on pixel values, and this makes visual interpretation easier and assist the human analyst. Histogram equalization is done on the image, where enhancement assigns more display values (or ranges) to the frequently occurring portions of the histogram.

Directional filtering is done on the panchromatic image of the year 2000 G. C. that has 12.5m spatial resolutions in order to enhance linear features along 0 and 20 degrees direction and subdues other features. This is used to perform mapping of geological structures (faults and lineaments) of the area. The angles used in the directional filter are based on the general orientation of the Ethiopian rift valley geological structures on the western rift margin and on measurements during field survey.

Image transformation

Image transformation is done mostly based on more than one band. Band ratio was done to remove differential illumination effect, which mostly results from shadowing. False color compositions were also used to map the degraded area on the composition of 465 for the year 1973 G. C. image and 743 for the years 1984 and 2000 G. C. images in RGB (Red, Green, and Blue) order. The band combinations are chosen based on the typical reflectance curves for three basic types of earth features, healthy green vegetation, dry bare soil, and clear lake water (Figs. 13) (adapted from Swain and Davis, 1978, in Lillesand, 2000).

On the MSS sensor of Landsat 1 of year 1973, false color composition of 465 is used:

Band 4 (with 0.5μm – 0.6μm wave length band width) gives red color and rock and soil have more reflectance on this bandwidth than vegetation and water body;

Band 6 (with 0.7μm – 0.8μm wave length band width) gives green color in false color composition and vegetations have a higher reflectance in this bandwidth than soil and water; and

Band 5 (with 0.6μm – 0.7μm wave length band width) gives blue color and in this bandwidth soils have higher reflectance than vegetations and water body (Figs.12 and 13).

Thus false color composite of image with 465-band combination in RGB order for degraded land results in light pink (pale violet) color.

On the TM and ETM+ sensors (that have the same band width) of Landsat 5 and 7 satellite images respectively, band combinations of 743 are used:

Band 7 (with 2.08μm –2.35μm wave length band width) gives red color and rock and soil have more reflectance on this bandwidth than vegetation and water body;

Band 4 (with 0.76μm – 0.90μm wave length band width) gives green color in false color composition and vegetations have a higher reflectance in this bandwidth than soil and water; and

Band 3 (with 0.63μm – 0.69μm wave length band width) which gives blue color in false color composite, in this bandwidth soils have higher reflectance than vegetations and water body (Figs. 12 and 13).

Thus false color composite of 743 band combination in RGB order for degraded land (bare soil) result in light pink (violet) color and it is more or less similar to the MSS 465 band combination in RGB order.

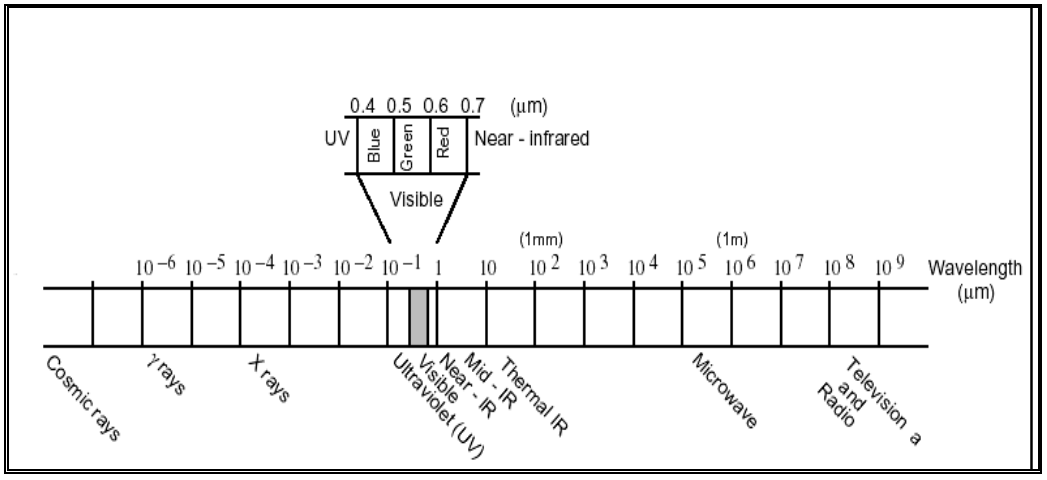

Figure 12. The electromagnetic spectrum (Lillesand, 2000).

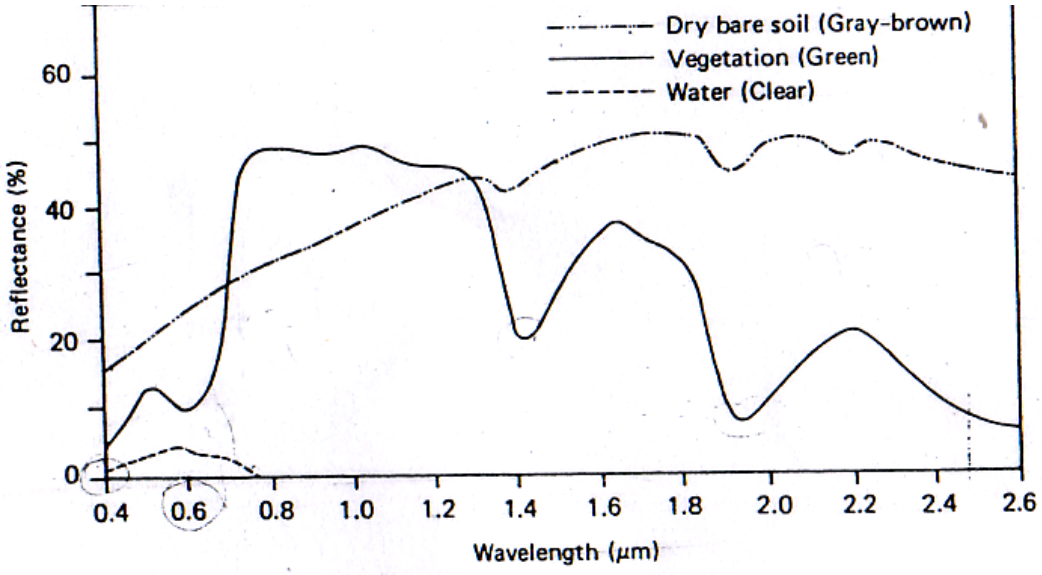

Figure 13. Typical spectral reflectance curves for three basic types of earth features (adapted from Swain and Davis, 1978, in Lillesand, 2000).

Other false color combinations in RGB order of bands 432 for Landsat 7 of ETM+ image were used for land use / land cover mapping. In this band combination open forest has brown to red color.

Image classification

Image classification depends on the brightness value of each pixel and it categorizes pixels of nearly the same values. Unsupervised classification was performed in order to have a general idea of the area.

4.3. GIS analyses

Geographic data is the combination of spatial (geometric) databases. Databases are descriptions about the geometric feature on the earth's surface. Inputs for the GIS analysis are from topographic maps, different available maps, Landsat satellite images of different years and SRTM data.

Different GIS analyses are done such as degraded area measurements, measurement of distance from drainage courses and geological structures, overlay analyses for evaluating land degradation rate and spatial variation, overlay of land degradation map with other environmental components in order to characterize the component based on site condition of degradation, weights and multi-criteria evaluation done on different environmental components in order to analyze the land degradation process in the study area, etc.

For the combination of different data layers that control the land degradation activity in the study area, all the data layers are converted to raster data sets having the same pixel size. Then for each data layer, reclassification, standardization, and weighting are performed in order to do multi-criteria evaluation, which is used to produce land degradation vulnerability map of the study area.

5. ASSESSMENT OF LAND DEGRADATION: RATE, AREAL EXTENT AND SPATIAL VARIATIONS

5.1. Introduction

Assessment of land degradation was done using remote sensing and GIS techniques integrated with field survey. The general degradation map of the study area (Fig. 14) was produced using satellite image of the year 2000 G. C. and false color combination of bands 743 in RGB order. It is recognized that intensely degraded lands appear light pink (light violet) on false color combination of bands 743 in RGB order and it is also verified during field survey. The fact that the image was acquired in January, a season during which many cultivated lands would not be covered by crops, has complicated the mapping of land degradation using digital interpretation, as these non-degraded cultivated lands also appeared to be light pink (light violet) on the image. As a result, careful visual interpretation supported by field survey data, followed by on screen digitization of the degraded lands was employed. The clearly defined (usually polygonal) shapes of the cultivated lands, which are mostly identified by the presence of some scattered trees on the fields, were also used to delineate the cultivated lands from the truly degraded terrains.

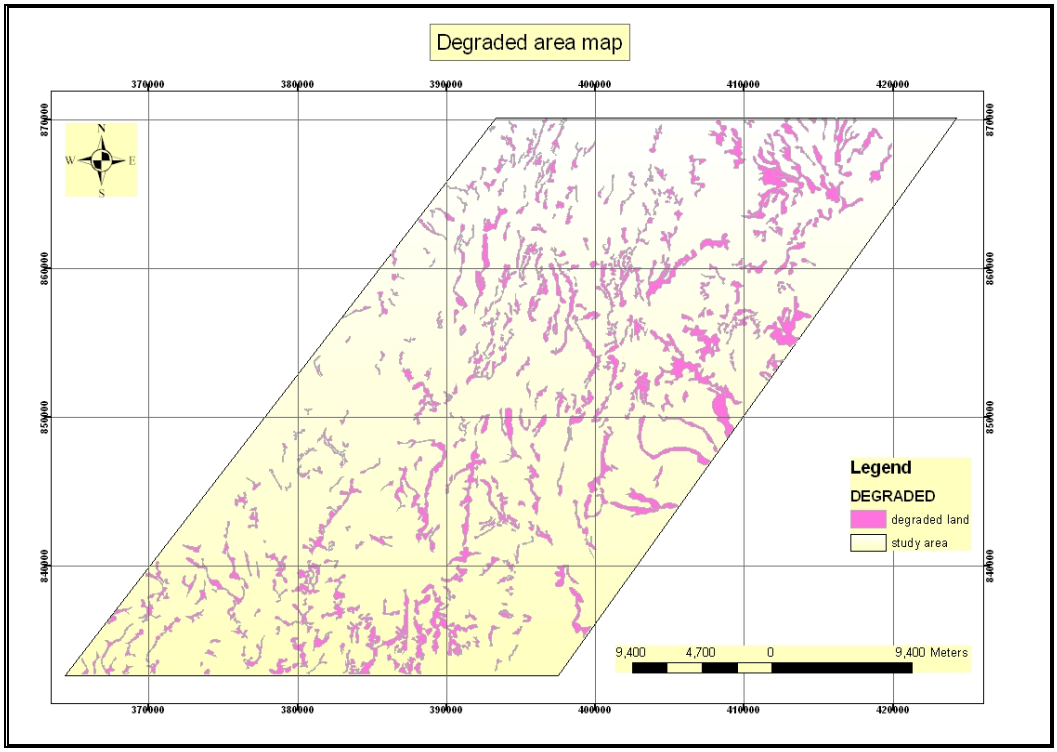

Figure 14. Study area degraded land map.

5.2. Time series/ change analysis

Satellite images of more than two different years are necessary for change detection analysis. Three Landsat satellite images that were taken in three different years have been, therefore, used for the assessment of the rate and spatial distribution of land degradation with time.

5.2.1. Rate and areal extent of land degradation

Assessment of the rate of land degradation was conducted on a selected sample area of about 247 square kilometers from the whole study area, using satellite images of the years 1973, 1984 and 2000 G. C. The sample area is selected based on the year

2000 G. C. image of false color composite of bands 743 in RGB order, which shows intense degradation in the selected area.

During this analysis:

1. The sample site was made to be the subset of the three different years' satellite images.
2. Color composite of bands 465 in RGB order on Landsat MSS image of year 1973 and 743 in RGB order on Landsat TM and ETM+ of the other two years' images were performed.
3. On screen digitization of degraded lands for each year was performed using ERDAS IMAGIN 8.6 software.
4. The ERDAS arc coverage vector layers were then changed to shape files in ArcView 3.2a software and one field was added to the table of each vector layer, and in this new field data type string values called "degraded area" was entered. This field makes the polygons of the degraded areas as one layer (figs. 15-17).
5. These layers have been imported to IDRISI 32 software where they were reclassified as raster of Boolean image of degraded area / non-degraded area (1/0) values, based on the field entered as degraded area on the database (figs. 18-20). On each of these raster layers, degraded and non-degraded areas were calculated using GIS analysis tool in IDRISI based on the two Boolean values. Then average rate of land degradation in areal base has been calculated from each year.

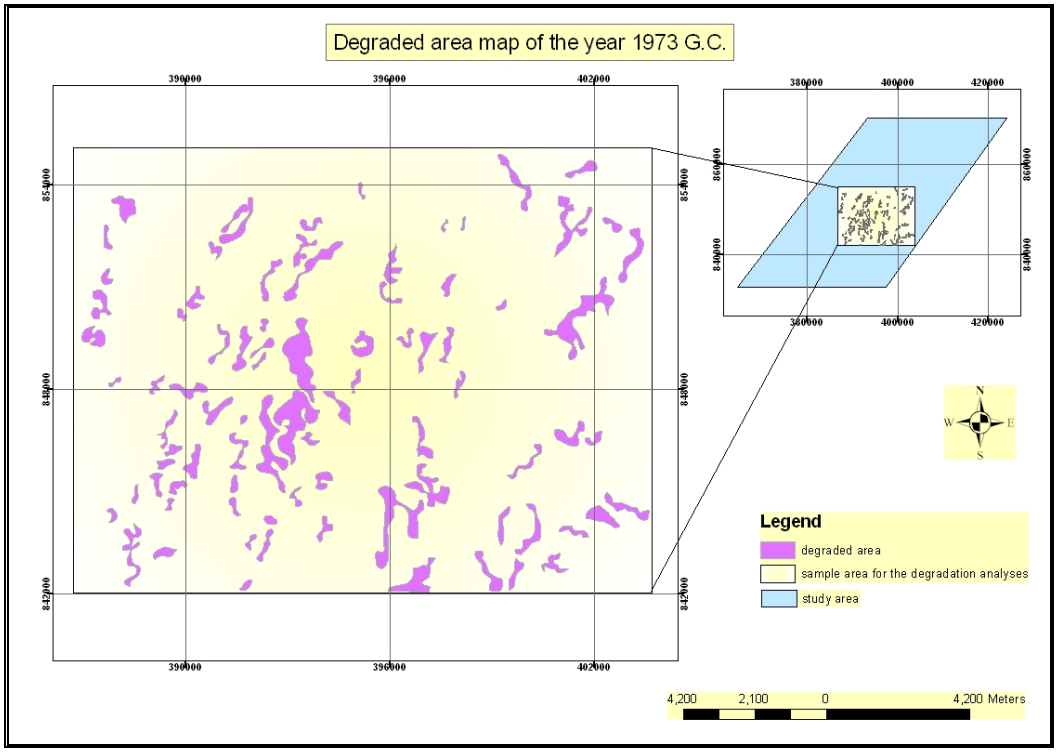

Figure 15. Degraded area map of year 1973 G. C.

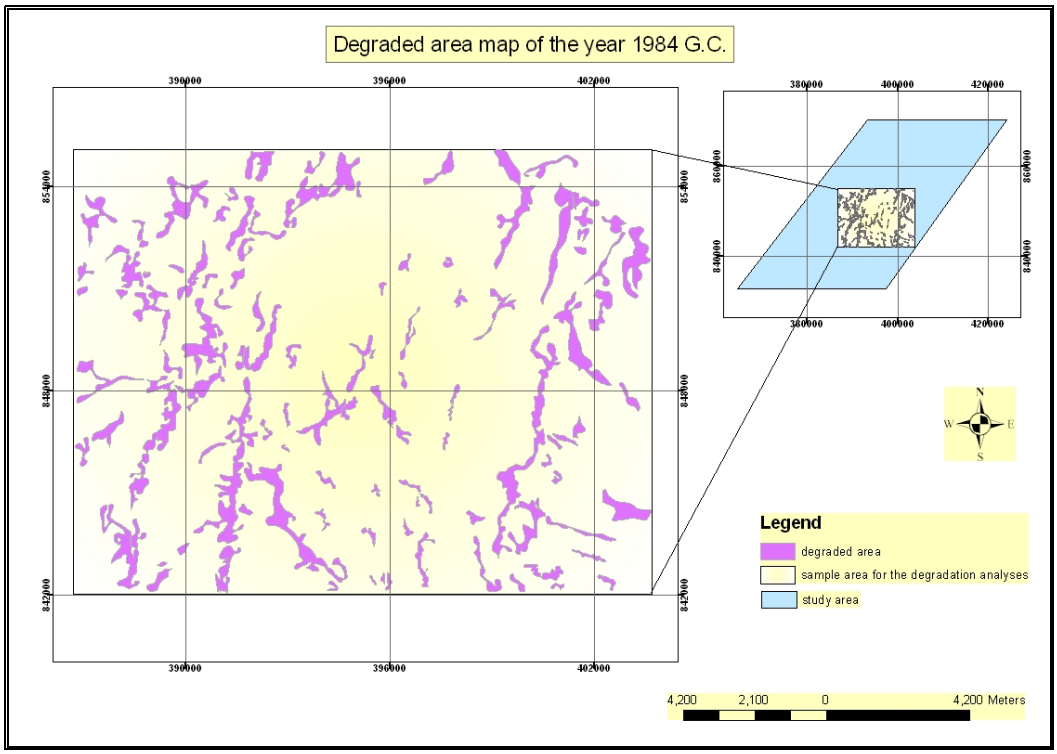

Figure 16. Degraded area map of year 1984 G. C.

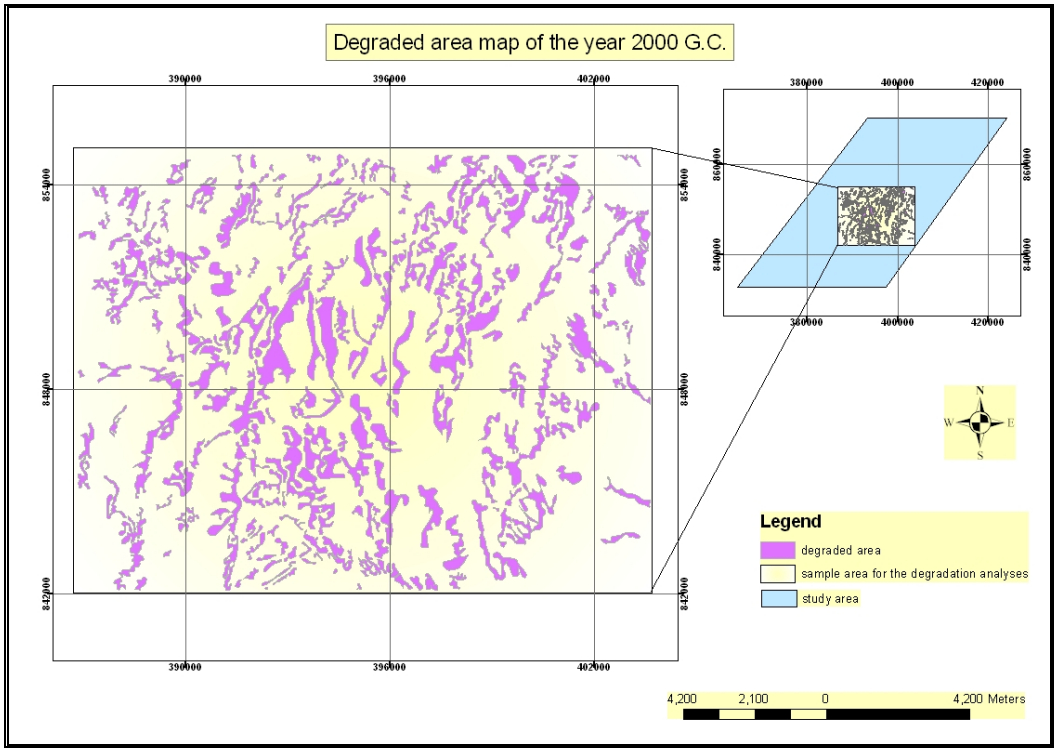

Figure 17. Degraded area map of year 2000 G. C.

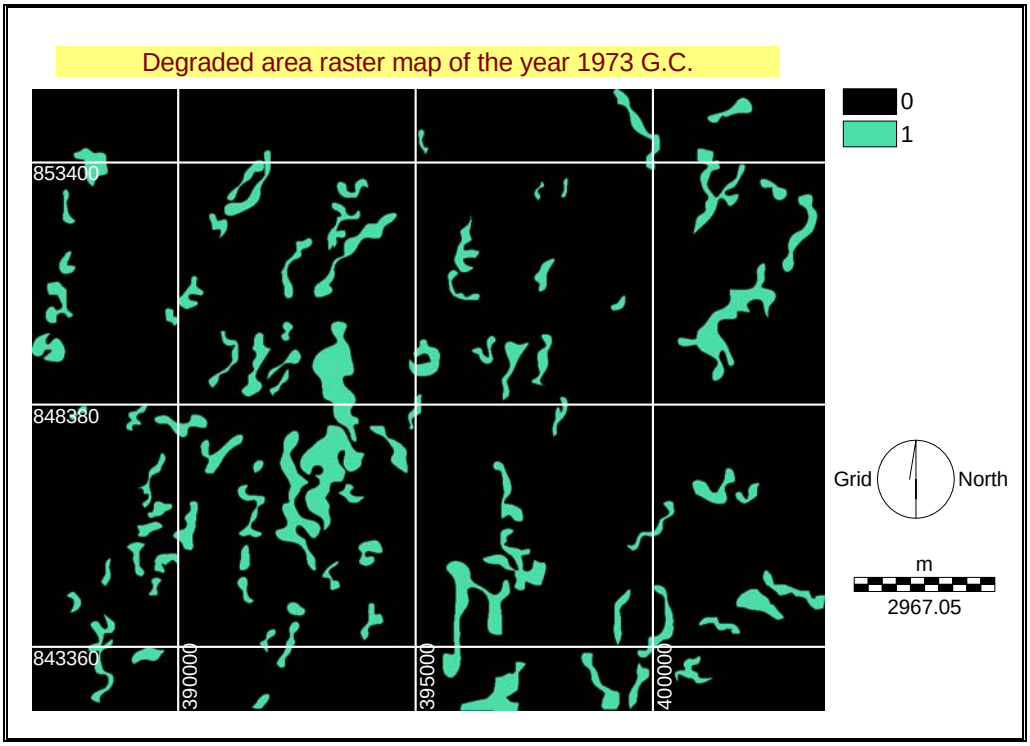

Figure 18. Raster Boolean map of degraded area (1) and non- degraded (0) of year 1973 G. C.

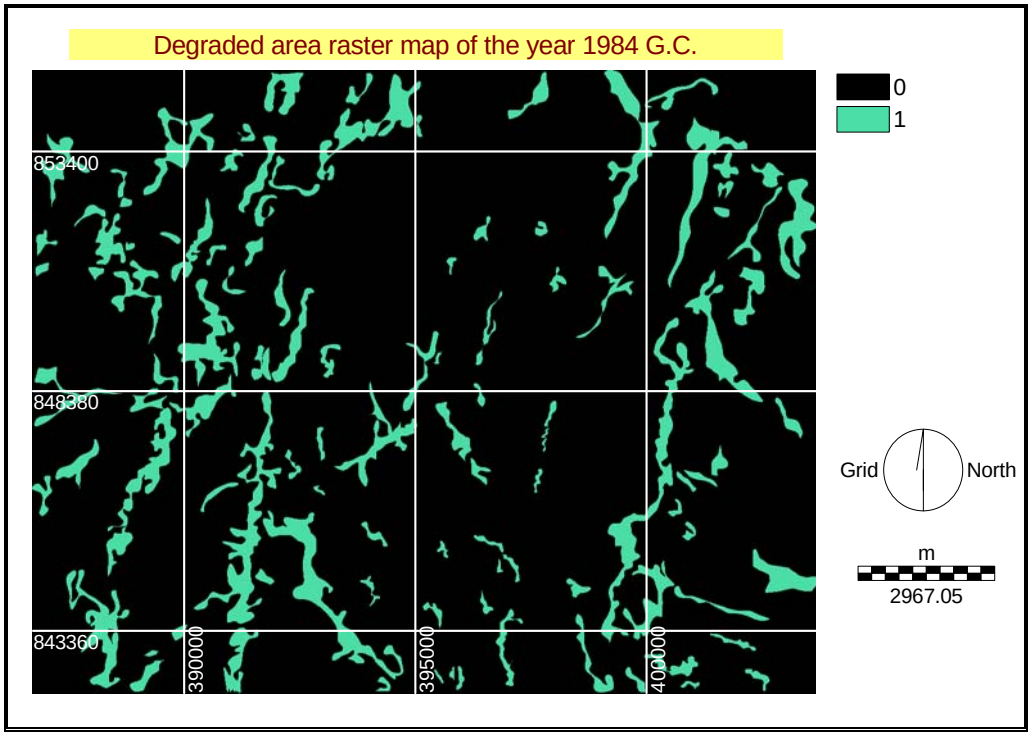

Figure 19. Raster Boolean map of degraded area (1) and non- degraded (0) of year 1984 G. C.

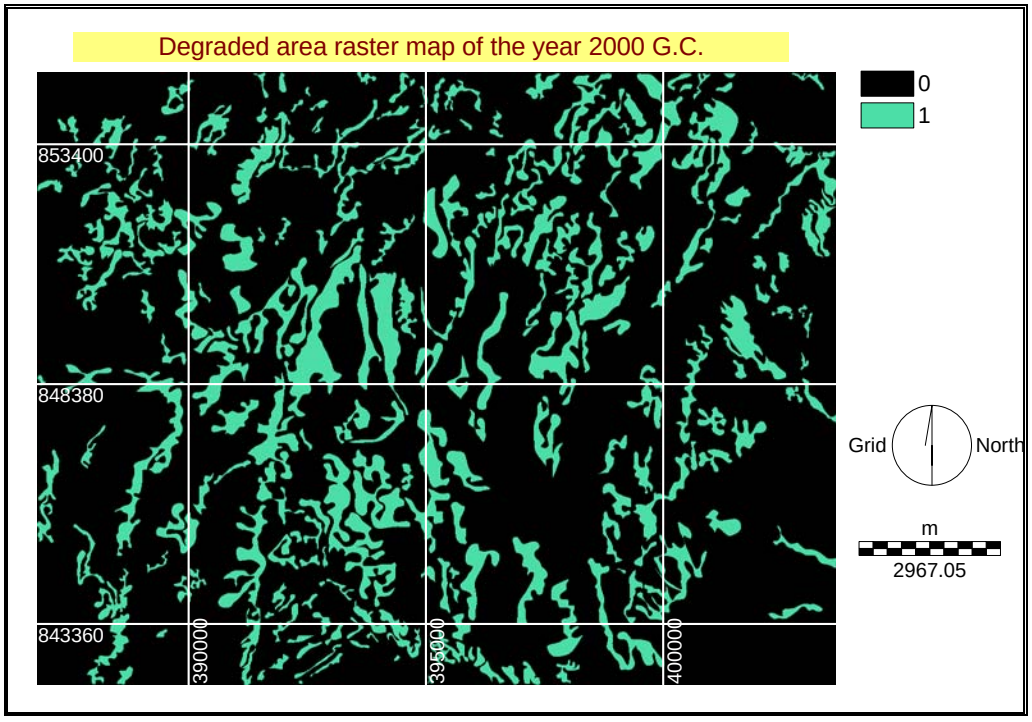

Figure 20. Raster Boolean map of degraded area (1) and non- degraded (0) of year 2000 G. C.

Table 2. Areas of the three years degraded and non-degraded lands and area in percent of degraded areas from the total sample site.

Year	Degraded areas (sq. Km.)	Non-degraded areas (sq. Km.)	Degraded areas (%)
1973	18.1	229.7	7.3
1984	25.8	222.0	10.4
2000	41.4	206.4	16.7

The analysis result (Figs. 15 – 20; Table 2) shows that the average rate of land degradation from year 1984 to 1973 is 0.7 square kilometers per year (25.8 - 18.1 Km^2 / 11 years) and from year 1984 to 2000, it was 1.0 square kilometers per year (41.4 - 25.8 Km^2 / 16 years). The result shows a general increasing trend of the rate of land degradation on an areal basis.

The areal extent is also increasing over time (Table 2). In the year 1973 G. C., 7.3 % was degraded, in the year 1984, 10.4 % was degraded and degraded area extended to 16.7 % in the year 2000 G.C.

5.2.2. Spatial variations of land degradation

To assess the spatial variation of land degradation with time in the study area, the small sample site and the Boolean images of the same three years, which were used in the rate of land degradation analyses, were used. Pair-wise comparisons using CROSSTAB module has been used in IDRISI between the Boolean raster pairs. In this analysis, the Boolean layers of two years were combined at a time using

OVERLAY operation and resulted in four classes of raster layer (Figs. 21 and 22; Tables 3-5).

Table 3. Classes that result from the pair-wise Boolean rasters of later year / earlier year, CROSSTAB overlay analysis.

Class	Later year	Earlier year
0 | 0	Not degraded	Not degraded
1 | 0	Degraded	Not degraded
0 | 1	Not degraded	Degraded
1 | 1	Degraded	Degraded

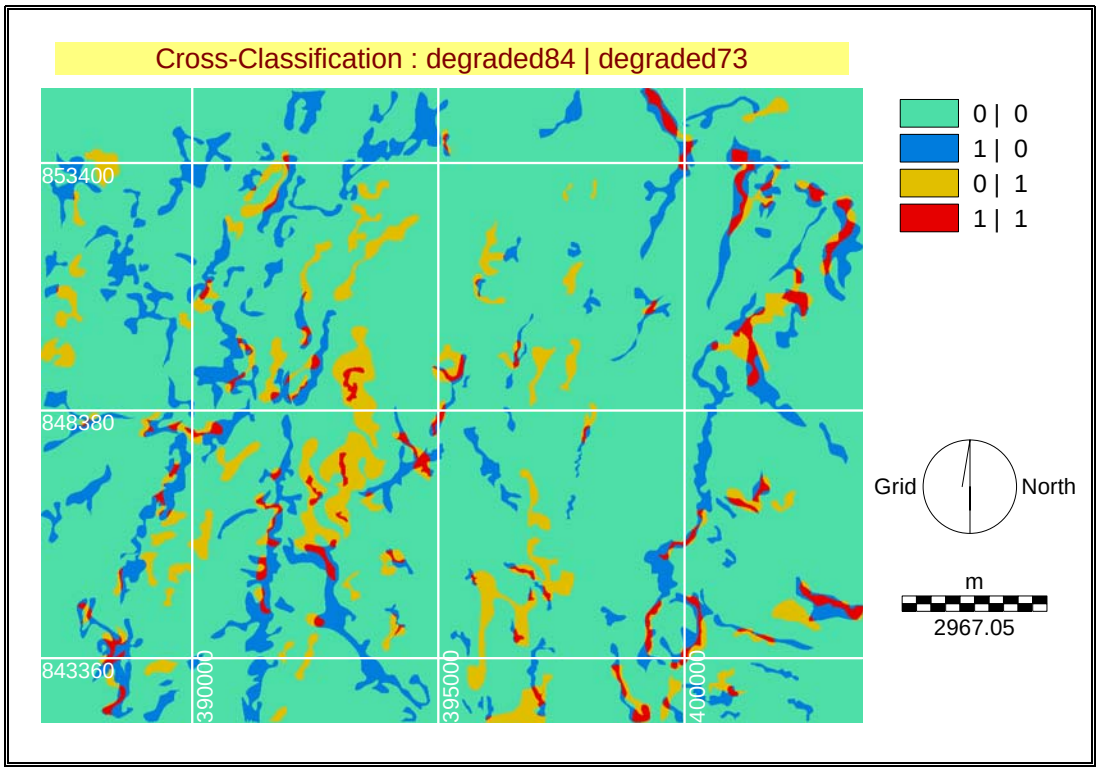

Figure 21. The pair-wise overlay Boolean images of year 1984 and 1973 G. C.

Table 4. Area calculated from classes that result from the pair- wise Boolean rasters of, year 1984 | year 1973, CROSSTAB overlay analysis.

Category	Area (Sq. km.)	Area (%)	Legend	Remark
1	208.9	84.3	0 | 0	Non degraded areas in both years
2	20.8	8.4	1 | 0	Degraded in 1984 and non degraded in 1973
3	13.8	5.6	0 | 1	Non degraded in 1984 and degraded in 1973
4	4.4	1.7	1 | 1	Degraded areas in both years

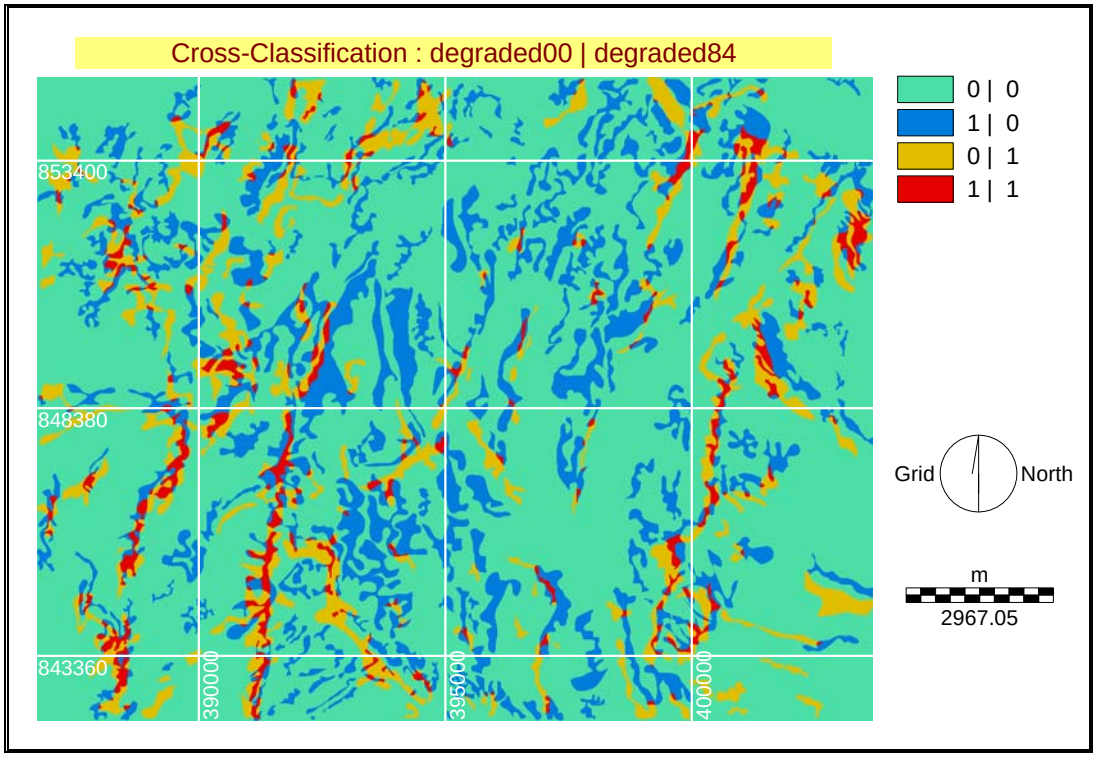

Figure 22. The pair-wise overlay Boolean images of year 2000 and 1984 G.C.

Table 5. Area calculated from classes that result from the pair- wise Boolean rasters of, year 2000 | year 1984, CROSSTAB overlay analysis.

Category	Area (Sq. km.)	Area (%)	Legend	Remark
1	186.0	75.0	0 | 0	Non degraded areas in both years
2	36.1	14.6	1 | 0	Degraded in 2000 and non degraded in 1984
3	19.5	7.9	0 | 1	Non degraded in 2000 and degraded in 1984
4	6.3	2.6	1 | 1	Degraded areas in both years

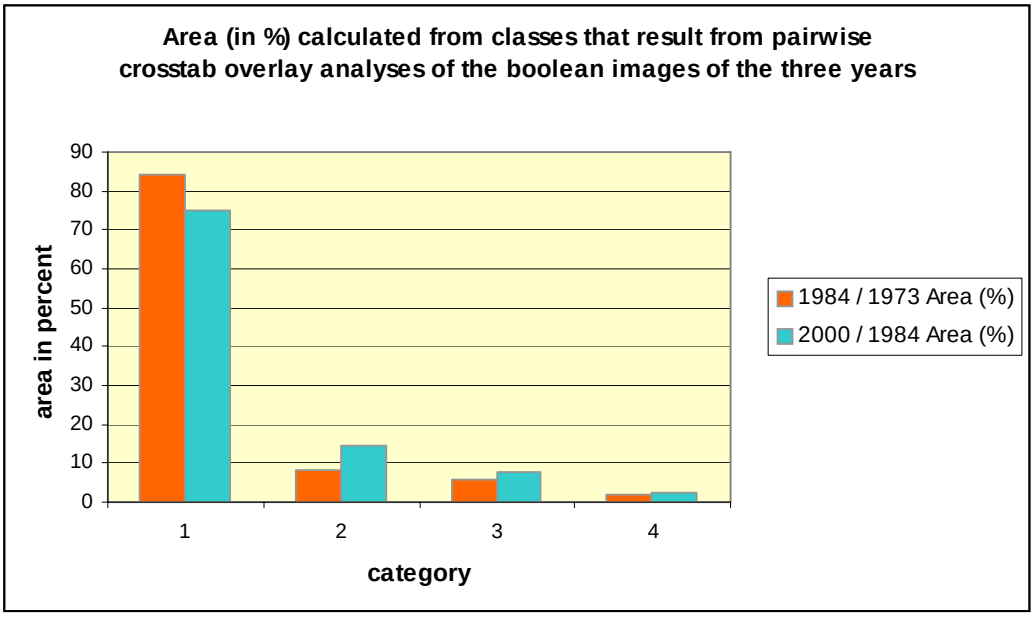

Figure 23. Area calculated from classes that result from the pair- wise Boolean rasters of, year 1984 | year 1973 and year 2000 | year 1984, CROSSTAB overlay analysis. Category 1 indicates Non-degraded areas in both years, category 2 indicates degraded in later year and non-degraded in earlier year, category 3 indicates non-degraded in later year and degraded in earlier year and Category 4 degraded areas in both years.

It must be noted that for the pair wise comparisons of the three years images, there is a differences in five years between the images. That is 1984/1973 have 11 years range and 2000/1984 was 16 years differences.

The amount of land, which was degraded, in 1984 that was not degraded in 1973 (areas represented by blue color on figure 21) is estimated to 8.4 % of the total area. The amount of land degraded in year 2000 that was not degraded in year 1984 (areas represented by blue color on figure 22) is estimated to 14.6 % of the total area. This shows expansion of existing and newly born degraded lands on other area is increasing over time and also the general land degradation amount is increasing over time (figs. 21-23 and tables 4 and 5).

In 1984/1973 G.C. estimated degraded area in the year 1984 and not degraded in the year 1973 (areas represented by blue color on figure 21) was 8.4 %, and area not degraded in 1984 and degraded in 1973 (areas represented by yellow color on figure 21) was 5.6 %: - this shows that 5.6 % was reclaimed or/and covered by vegetations and 8.4 % was due to the expansion of existing degraded land or the creation of newly degraded land on other areas, hence it was found out that, the degraded land was increasing by 2.8 % (8.4 - 5.6 %) than the vegetated or reclaimed land. This increasing of degraded land in areal bases was rising to 6.7 % (14.6 – 7.9 %) from the vegetated or reclaimed land on 2000/1984 G.C. that is for 2000/1984 G.C. estimated area of degraded land in 2000 and which was not degraded in 1984 (areas represented by blue color on figure 22) was 14.6 % and area not degraded in 2000 and which was degraded in 1984 was 7.9 % (areas represented by yellow color on figure 22) (tables 4 & 5).

It is estimated that the amount of degraded area during both years (areas represented by red color on cross classified images on figure 21 &22) of 1984/1973 was 1.7 % and increased to 2.6 % in 2000/1984 G.C. This also shows the general increasing trend of the degraded lands.

From the resulting raster layers of the two analyses (Figs. 21-23; Tables 4-5), it can be established that areas that did not degraded on both analyses have been decreasing, existing degraded lands are expanding and also newly born degraded lands on other areas have also been observed and generally the amount of degraded areas show an increasing trend from earlier years to later years on both analyses.

6. **LAND DEGRADATION ACTIVITY**: ASSESSMENT AND GIS ANALYSES

6.1. Introduction

One of the major objectives of this study is to generate land degradation vulnerability map of the study area based on various interrelated components of the environment using integrated techniques of remote sensing, GIS and field survey. These interrelated components are used as factor (input) data sets for the land degradation analysis process. Input data sets were selected based on their globally established impact on land degradation activity and on locally significant factors established based on specific field observations. The data sets considered as inputs are verified to be operational (have some relation with the land degradation activity), complete (full information about the input data is available), measurable in any scale, variable (non uniform) in the area, and it is not repeated (non redundant).

Six steps have been followed in producing the susceptibility map:

1. Selection of the data sets to be used as inputs. Input data sets were selected based on locally significant factors established based on field observations and on their globally established impact on land degradation activity.

2. Each factor map is produced from remote sensing data, topographic maps and different available maps.

3. Rasterization of the produced data sets. The data sets must be in the same data model. Vector data layers were changed to raster data layers, in order to perform different GIS analyses between data layers such as cross-tabulation and overlay analysis. IDRISI software performs most analyses on raster data, hence rasterization of vector data layers was done based on the only raster layer, that is DEM of the study area, of pixel size 90m.

4. Appropriate analysis addressing the degradation activity was done for each raster data set based on observations in the field and using the general land degradation map of the study area. For example, slope angle derivation from the elevation raster, distance map production from the geological structure map, etc. In this process, new information is gained by generating new maps from existing maps.

5. Standardization of different factors to the same scale before combining them. Typical and simple standardization using the minimum and maximum values as scaling points called linear scaling is used according to the minimum and maximum capacity of the computer or standardizing options on the used soft wares. For example, IDRISI gives standardization options of 0 –1 (real number scale) or 0 – 255 (byte scale). The byte scale is usually recommended because the multi-criteria evaluation module has been optimized for speed using a 0 – 255 level standardization. Therefore, standardization of each data set to a common scale of 0 – 255 (assigning higher values to more susceptible attributes) is adopted here, in order to combine all those with the same scale.

6. Assigning weights for each controlling factor and combining datasets depending on their weight. The final combined result gives land degradation susceptibility map of the study area. This susceptibility map is further classified in order to generate land degradation vulnerability map. The land degradation vulnerability map is finally verified by GPS point data that are taken on degraded areas during field survey.

Based on the assessment of land degradation process in the study area using field survey, the selected input data sets are drainage, slope, geological structure, geology, soil and land use / land cover. As it is examined, these six environmental components have a strong relationship and effect on the land degradation activity in the study area. Although rainfall is known to have strong triggering effect on land degradation process, its effect is nearly the same for such small area. As a result the rainfall data are excluded from the data set.

6.2. Land degradation controlling factors and GIS analysis

6.2.1. Land degradation distribution map

The general land degradation map (Fig. 24) is overlain on each factor map to see in which areas land degradation is intense and to characterize each class of the factor map based on the land degradation intensity in each class.

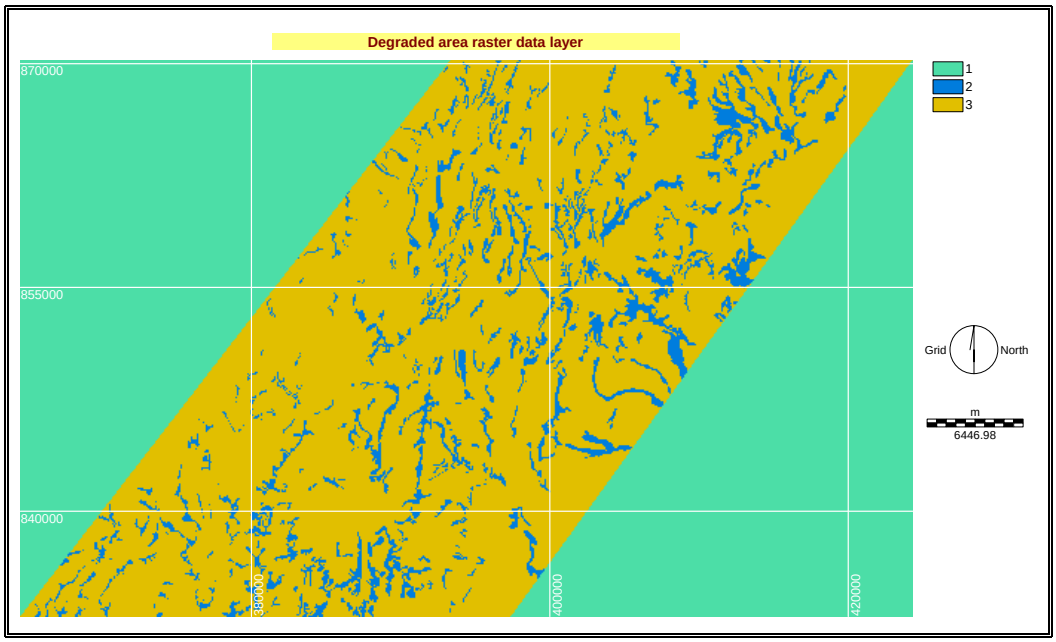

Figure 24. Land degradation map of the study area. Class 3 is non-degraded land in the study area; Class 2 is highly degraded land; and class 1 is out of the study area.

For multi-criteria evaluation, the constraint data layer and the factor data layers, that have a relationship with land degradation in the study area, are used.

6.2.2. Constraint data layer

A constraint serves to limit the alternatives under consideration. In this case, the study area is the constraint for the analyses. Areas excluded from consideration are outside the study area and those opened for consideration are inside the study area (Fig. 25).

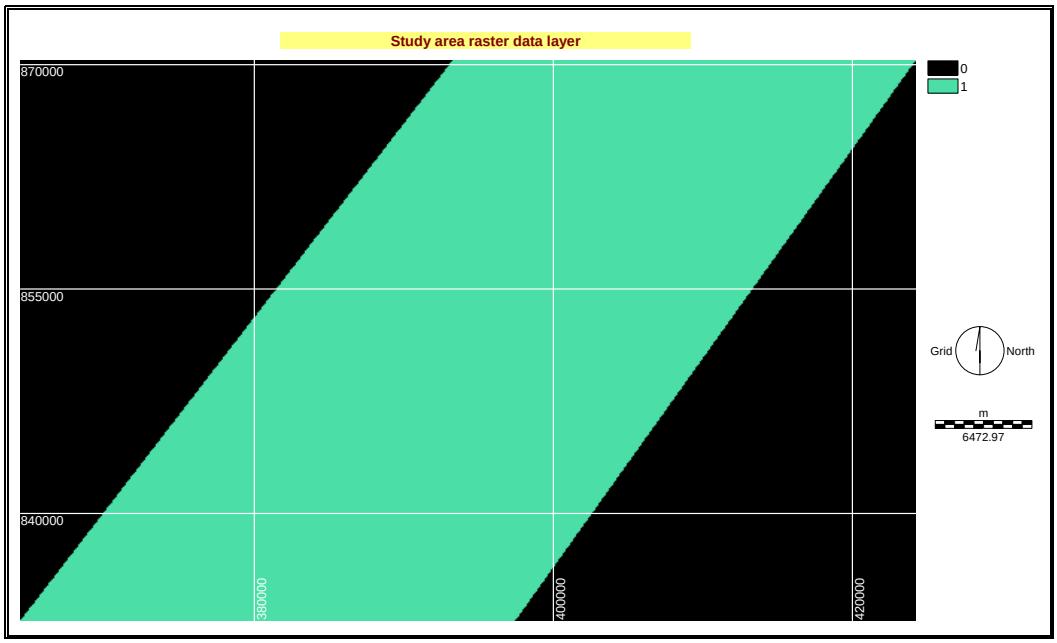

Figure 25. Study area as Boolean constraint data layer.

6.2.3. Factors that control land degradation in the study area

These factors have certain link with the land degradation process and they increase or decrease the susceptibility of areas to land degradation activity.

Geological structures

The study area is tectonically active and it is affected by geological structures in the form of major and minor normal faults, joints and fractures. The faults produce steep escarpments converted to high slopes where erosion and land degradation is intense. Most faults and fractures in the area follow a general North-South orientation, and most drainage lines follow these structures. Intense land degradation features are observed along these structures. Generally, land degradation activity decreases away form the structure increases. Therefore, distance analysis is performed on the geologic structure map (Fig. 26).

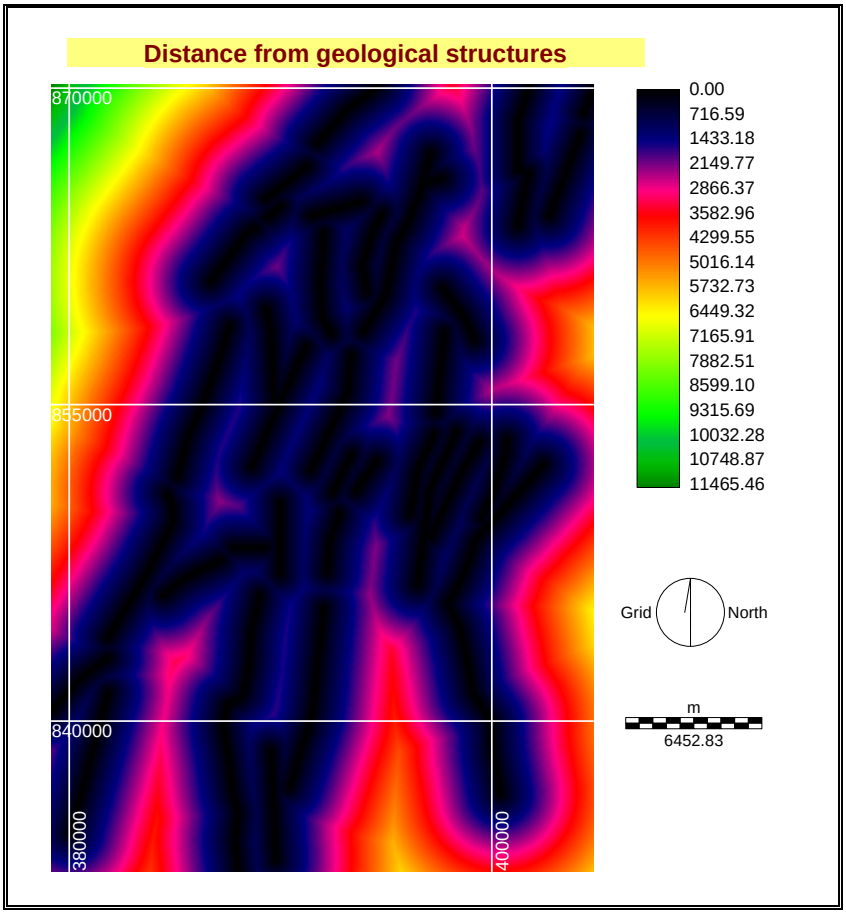

Figure 26. Distance derived from geological structures.

Slope angle (geomorphology)

It is observed that erosion and land degradation activity increases with increasing slope angle. Therefore, high slope areas are relatively more vulnerable to land degradation than low slope areas. In the study area slope formation is mostly related to underlying geological structures, volcanic domes and river gorges, which by themselves follow major structural lines. The maximum slope in the study area, as calculated from the DEM, is 65 degrees (Fig. 27).

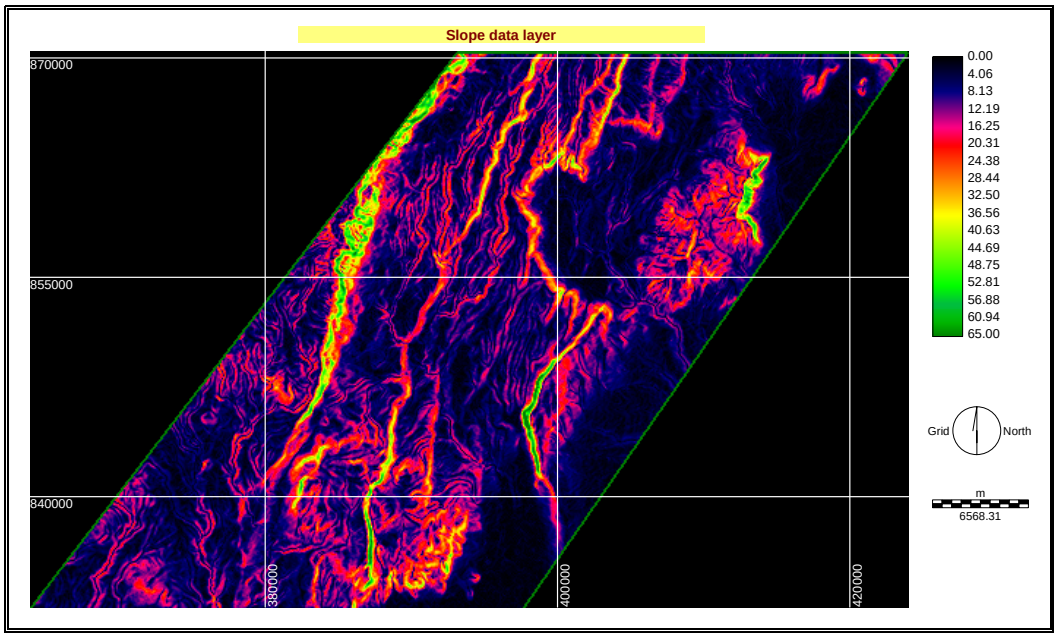

Figure 27. Slope map expressed in degrees.

Drainage

In the study area, it is observed that land degradation is intense along drainage lines. River gorges produce slopes, which are affected by intense erosion. Lateral erosion along riverbanks is also facilitated by the weak nature of the underlying geological materials. Accordingly, it is generally considered that land degradation decreases away from drainage lines (Fig. 28).

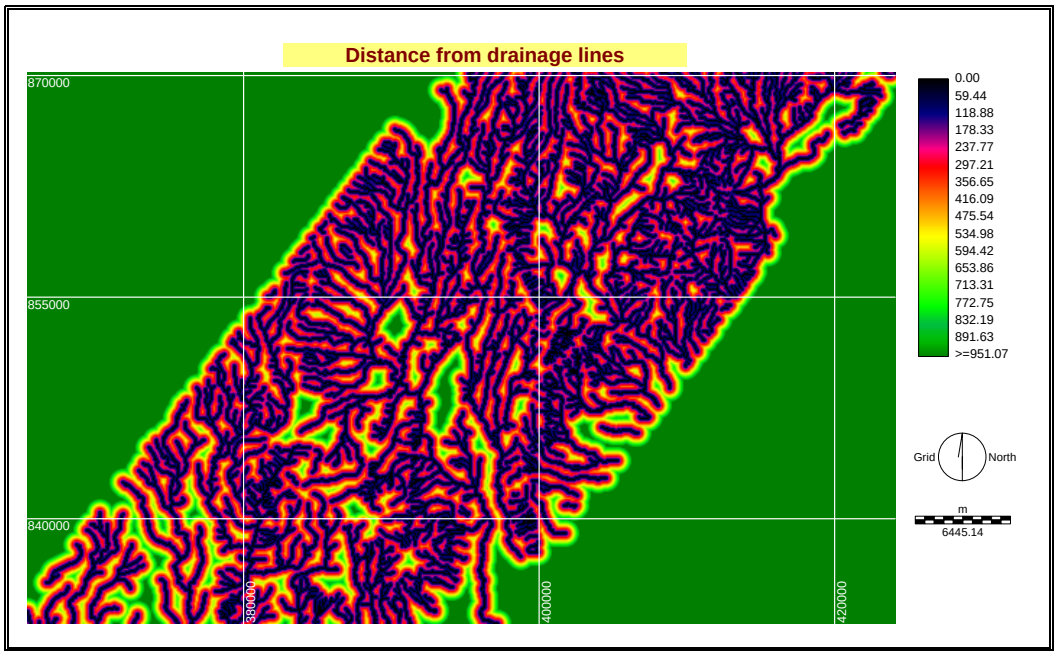

Figure 28. Distance from drainage lines.

Geology (lithology)

The major lithologies constituting the study area are (Fig. 29):

1. ignimbrite and tuff unit (rift floor ignimbrite) that covers large area and has a repetitive succession of ignimbrite, ash, pumice and tuff layers;
2. felsic volcanoclastic formation; and
3. rhyolite and associated obsidian flows.

All the lithologies are affected by erosion but the ignimbrite and tuff unit is highly degraded compared to the other two units. The rhyolite unit is the least degraded.

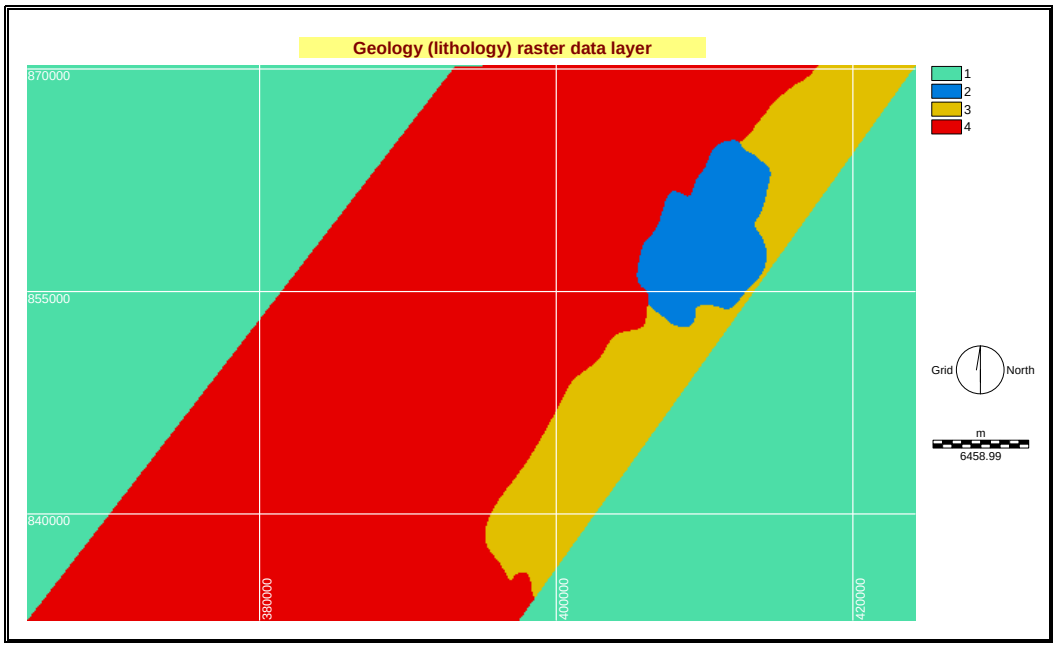

Figure 29. Raster geology data layer. Class 1 is out of the study area, class 2 is the rhyolite unit, class 3 is the volcanoclastic formation and class 4 is the ignimbrite and tuff unit.

Land use / land cover

The sensitivity of each land use / land cover class for land degradation in the study area was calculated based on the general land degradation map. For this analysis, land degradation data layer of the study area was cross-tabulated with land use / land cover data layer using CROSSTAB module in IDRISI 32 software. Then using AREA module, the degraded area in each land use / land cover class was calculated. To compare the amount of degraded area in each class, the total degraded area in each land use / land cover class was divided to the total area of the respective land use / land cover class and the result was multiplied by 100 in order to get area of degraded lands in percentage of each class (Table 6). Based on the size of degraded lands in % of each class, new classes were re-assigned for each land cover classes. These new

class numbers are used to standardize the land use / land cover data layer (Figs. 30 and 31).

Table 6. Method used for the reclassification of land use/ land cover data layer based of the study area on the amount of degraded land in % of each land use/ land cover class.

Each class of land use/ land cover	**Total area of each class (Sq. Km.)**	**Classes created during CROSSTAB**	**Area of degraded lands in each class (sq. km.)**	**Area of degraded lands in (%) of each class (New class assigned)**
7 (cultivated land (annual) & perennial)	504.86	1/1	48.62	9.63
1 (water body)	0.56	1/2	0.00	0.00
11 (cultivated land, grass land, bush & shrub)	57.49	1/3	12.75	22.18
3 (cultivated land)	35.87	1/4	0.89	2.48
6 (town)	8.58	1/5	0.74	8.63
8 (cultivated land, bush &shrub)	357.73	1/6	47.41	13.25
10 (grass land)	59.64	1/7	12.82	21.50
9 (cultivated land & grass land)	48.44	1/8	7.34	15.15
5 (cultivated land (int.))	35.51	1/9	2.93	8.25
2 (wet land)	20.53	1/10	0.40	1.95
4 (open forest)	70.33	1/11	3.71	5.28

From this result land use/ land cover class that is cultivated land mixed with grassland, bush and shrub is intensely affected by land degradation.

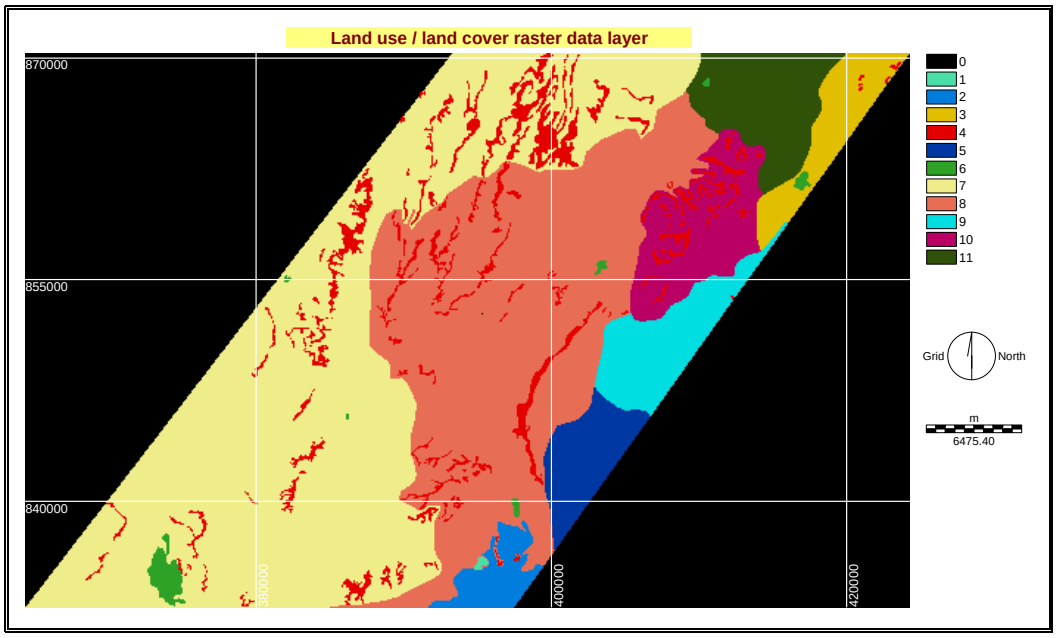

Figure 30. Land use / land cover raster map of the study area.

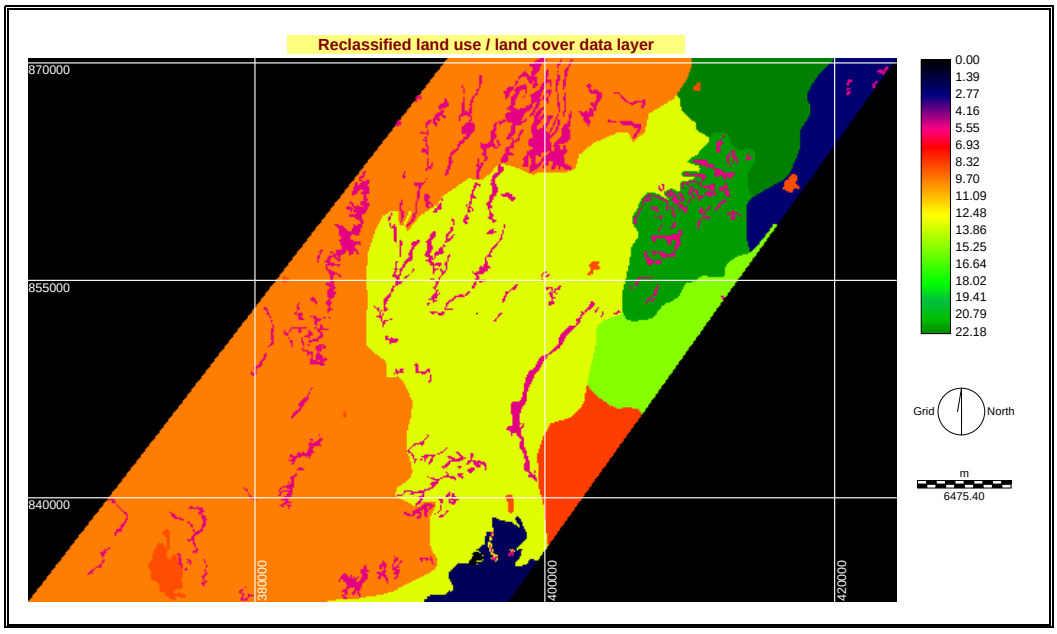

Figure 31. Reclassified land use/ land cover map of the study area (Based on the size of degraded lands in % of each land use/ land cover class (table 6)).

Soil

To characterize the study area soil types depending on onsite nature of their resilience and sensitivity to land degradation and erosion, soil data layer was cross-tabulated with the general land degradation map of the study area. Then similar procedures as for land use / land cover data layer were followed and the results are indicated in Figs. 32 and 33 and Table 7.

Table 7. Method used for the reclassification of soil data layer based of the study area on the amount of degraded land in % of each soil class.

Each class of soil type	**Total area of each class (sq. Km.)**	**Classes created during CROSSTAB**	**Area of degraded lands in each class (sq. km.)**	**Area of degraded lands in (%) of each class**
1 (calcic xerosols)	46.07	1/1	8.31	18.04
2 (chromic luvisols)	0.01	1/2	0.00	0.00
3 (chromic vertisols)	145.46	1/3	22.20	15.26
4 (eutric cambisols)	37.63	1/4	2.43	6.46
5 (eutric fluvisols)	122.18	1/5	14.89	12.19
6 (eutric nitisols)	18.71	1/6	2.33	12.45
7 (leptosols)	61.89	1/7	3.88	6.27
8 (no data)	3.79	1/8	0.24	6.33
9 (no (thin) soil)	19.67	1/9	3.04	15.46
10 (orthic solonchaks)	547.67	1/10	61.69	11.26
11 (pellic vertisols)	64.72	1/11	6.27	9.69
12 (vitric andosols)	131.11	1/12	12.22	9.32

From this analysis calcic xerosols soil type is intensely degraded than others. Xerosols are acidic soils (Office of Arid Lands Studies, 2001).

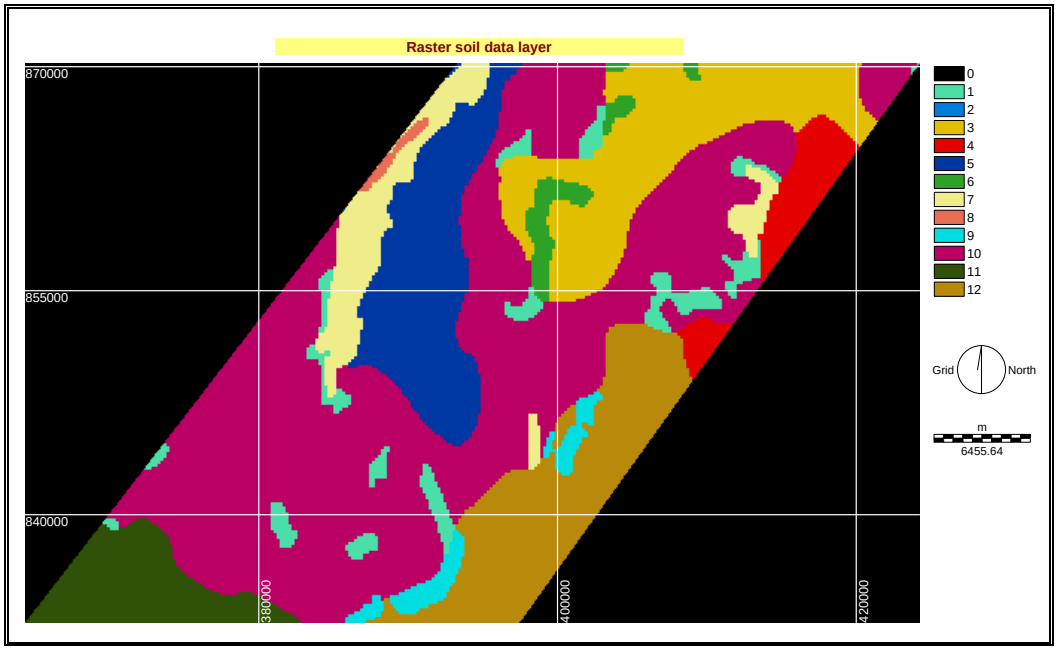

Figure 32. Raster soil map of the study area.

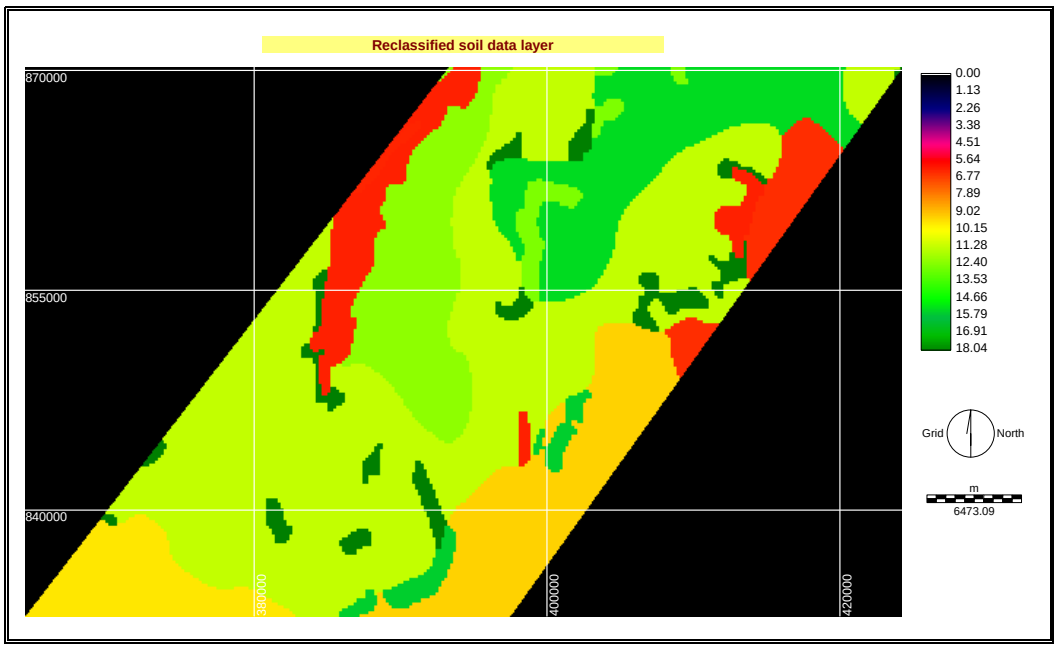

Figure 33. Reclassified soil map of the study area (based on the size of degraded lands in % of each soil class).

6.3 Normalization (standardization) of factor maps

The above data layers, which are reclassified based on their relationship with land degradation process, have their own measuring values such as slope in degrees and distance in meter. Therefore, it is necessary that the controlling factors must be standardized before combining them for producing a single data layer of susceptibility to land degradation, in order to relate each data layer with the land degradation process.

Standardized values of a set of rasters assigned to a common numeric range reflecting only the range of land degradation susceptibility. Low values show low degradation and high values high degradation.

Factor maps can be classified on the basis of the type of information available as deterministic or fuzzy. This classification is related to the distinction between the existence of defined and non-defined boundary (Malczewski, 1999). Deterministic data layers in this analysis are geology, land use/ land cover and soil that have definite boundary between classes. Fuzzy data layers are slope, proximity to structures and proximity to drainage lines, which do not have well defined boundary.

IDRISI software offers a built in decision support module for performing multicritera decision analysis. Fuzzy module in IDRISI 32 software was used for the standardization of distance data layers of drainage and geological structures, and slope data layer (Figs. 34-36). For drainage and structure a monotonically decreasing module was used because as distance from geological structures, and drainage lines

increases land degradation effect decreases. For slope monotonically increasing module was used because as slope increases land degradation effect also increases. On the other hand, for the reclassified soil, land use / land cover and geology data layers, standardized using STANDARD module in IDRISI 32 software (figs. 37-39), result in a common scale of values with other data layers.

Therefore, standardization of each dataset to a common scale 0 – 255 (giving higher values to more susceptible attributes) is performed here, in order to combine all those have the same scale.

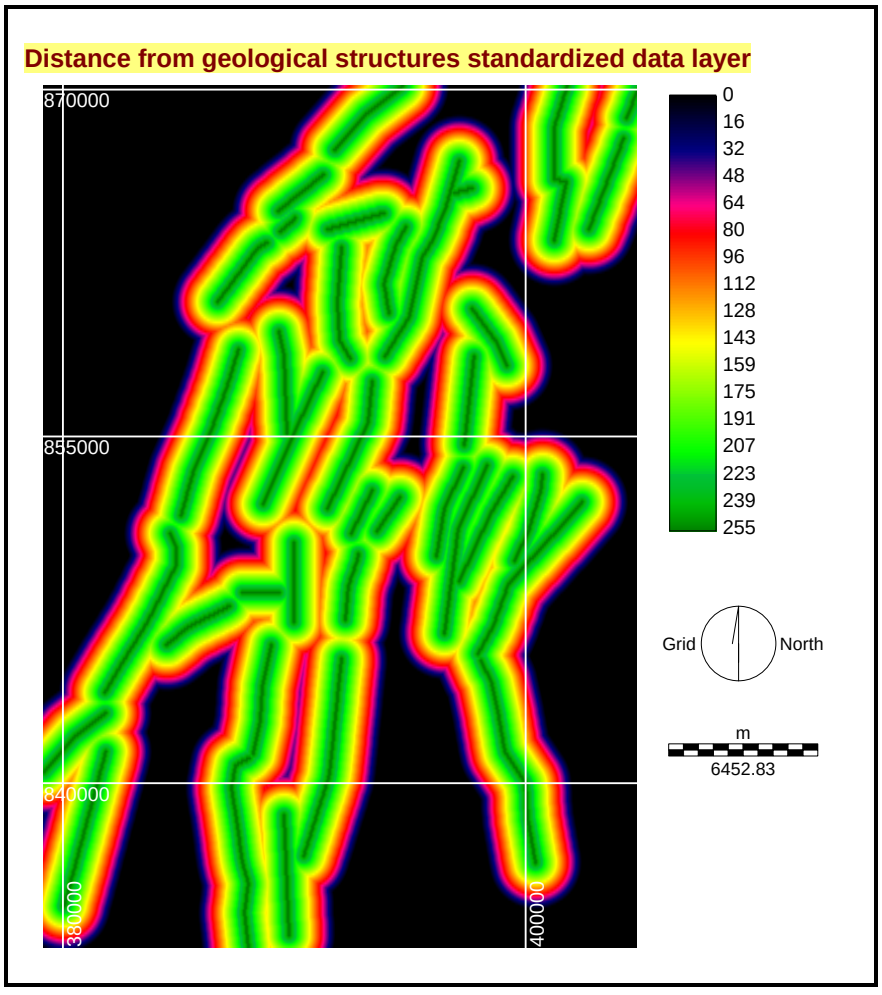

Figure 34. Data layer that shows proximity to geological structures.

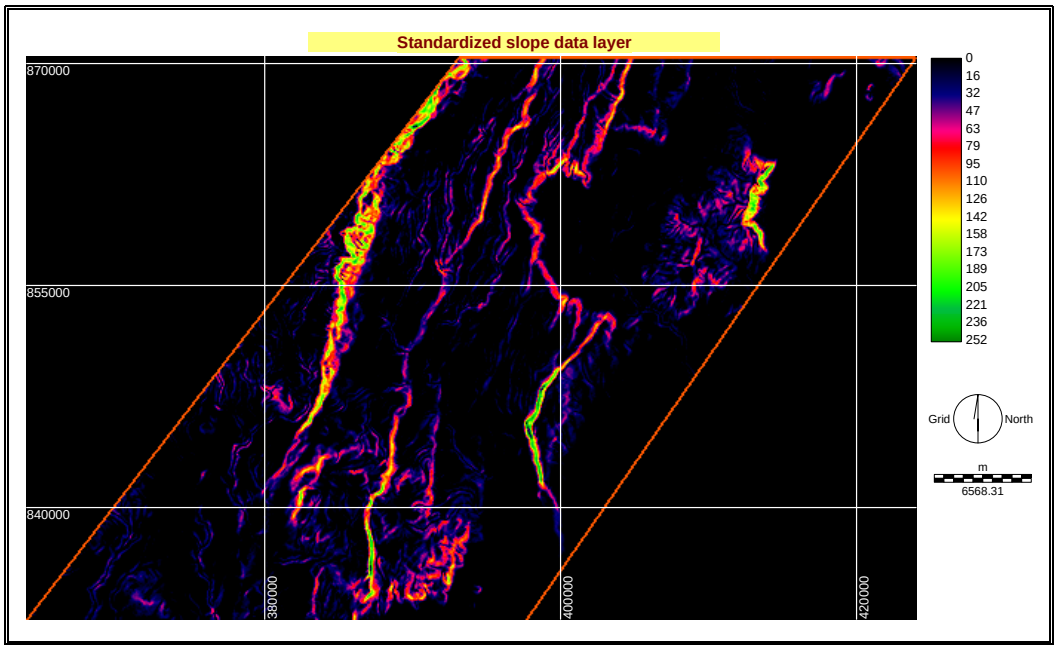

Figure 35. Standardized slope data layer.

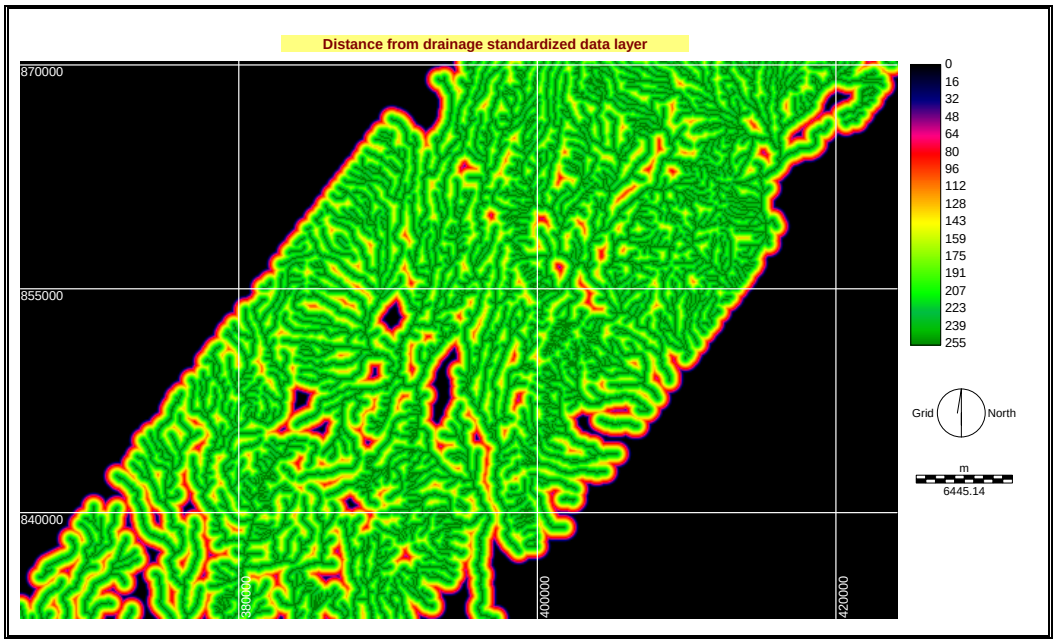

Figure 36. Data layer that shows proximity to drainage lines.

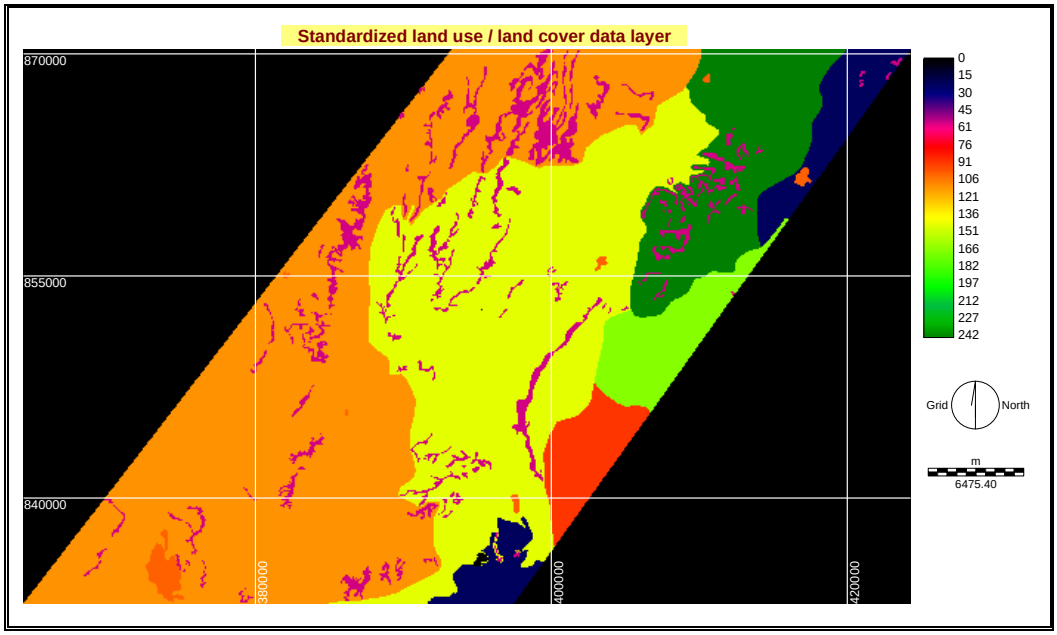

Figure 37. Standardized land use / land cover data layer.

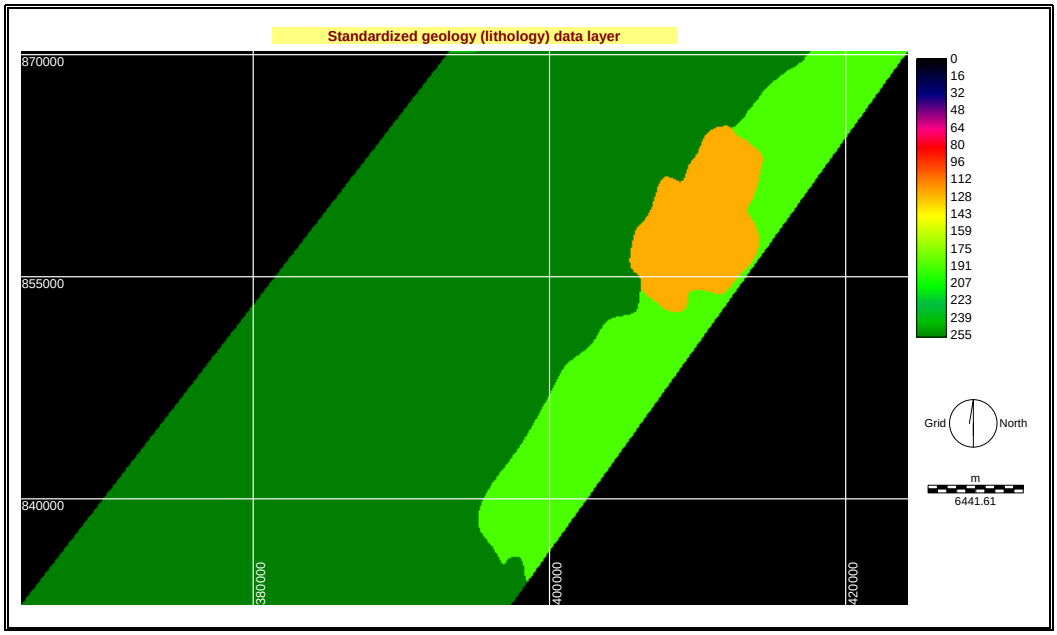

Figure 38. Standardized geology data layer.

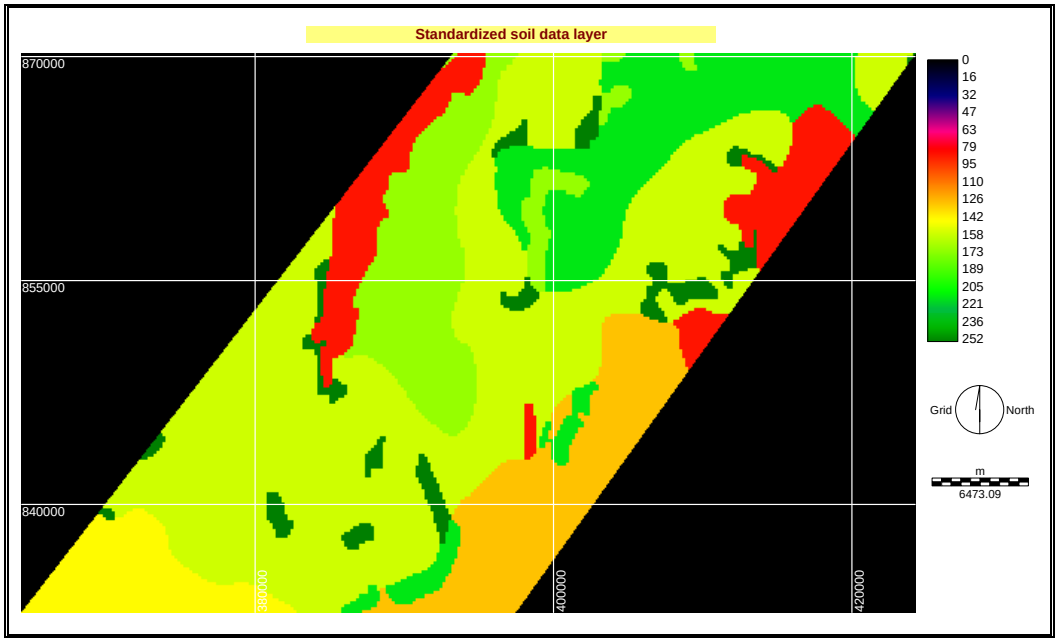

Figure 39. Standardized soil data layer.

6.4 Weight of factor maps

After the standardization (normalizing the measuring scales) of each controlling factor, weight is given for each layer based on pair-wise comparison of two data layers at the same time, using pair-wise comparison of 9-point continuous rating scale in IDRISI 32 (table 8). Weighting is used to express the relative importance of each factor relative to other factor. The larger the weight the more important is the factor in overall utility.

Pairwise comparison method was developed by (Saaty (1980) in Malczewski, 1999) in the context of the analytic hierarchy process (AHP), it takes as an input the pair wise comparison and produces the relative weights as output. One advantage of the pair wise comparison method is that only two criteria have to be considered at a time

and this method has been tested theoretically and empirically for a variety of decision situations (Malczewski, 1999). IDIRSI software automates to produce weights using analytic hierarchy process of pairwise comparison method.

Table 8. Pair-wise comparison, 9-point continuous rating scale (adapted from Saaty, 1980, in Malczewski, 1999).

Intensity of importance	**Definition**
1	Equally important
1/2	Equally to Moderately Less important
1/3	Moderately Less important
1/4	Moderately to Strongly Less important
1/5	Strongly Less important
1/6	Strongly to Very strongly Less important
1/7	Very strongly Less important
1/8	Very strongly to Extremely Less important
1/9	Extremely Less important

The relative comparisons between the six data layers were performed based on iteration of the layers and verified by field GPS point data layer taken on degraded lands. The various comparisons conducted indicated that highest weighting for the drainage data layer followed by the slope data layer, geological structure data layer, geology data layer, soil data layer and land use/ land cover data layer results in a susceptibility map that reflects the real ground conditions verified in the selected study site.

Based on the given pair-wise comparison, IDRISI calculates hierarchical weights for all layers (Fig. 40). It also calculates consistency ratio that shows if the given pair-wise weights are accepted or if another arrangement is necessary.

	drainage3	slope12	geostructure2	ageology13	soil41	landcover2
drainage3	1					
slope12	0.5	1				
geostructure2	0.3333	0.5	1			
ageology13	0.25	0.3333	0.5	1		
soil41	0.2	0.25	0.3333	0.5	1	
landcover2	0.1667	0.2	0.25	0.3333	0.5	1

```
The eigenvector of weights is :

        drainage3 : 0.3825
          slope12 : 0.2504
    geostructure2 : 0.1596
       ageology13 : 0.1006
           soil41 : 0.0641
       landcover2 : 0.0428



Consistency ratio =    0.02
Consistency is acceptable.
```

Figure 40. Weight of factors that control land degradation process in the study area: the pairwise ratio matrix (left), the module result of the eigenvector of ratio matrix that gives weight for each factor (right).

6.5 MCE (Multi-Criteria Evaluation)

For the assessment of land degradation activity in the study area, the selected six criteria were evaluated following a procedure called multi-criteria evaluation (MCE), which in this case is achieved by weighted linear combination (WLC). The weighted linear combination analysis takes into consideration all data layer values depending on their weight.

Weighted linear combination (WLC) **result** = ((factor **1*** weight **1**)+ (factor **2*** weight **2**)+ (factor **3*** weight **3**)+ (factor **4*** weight **4**)+ (factor **5*** weight **5**)+ (factor **6*** weight **6**)) * **constraint** (fig 41a)

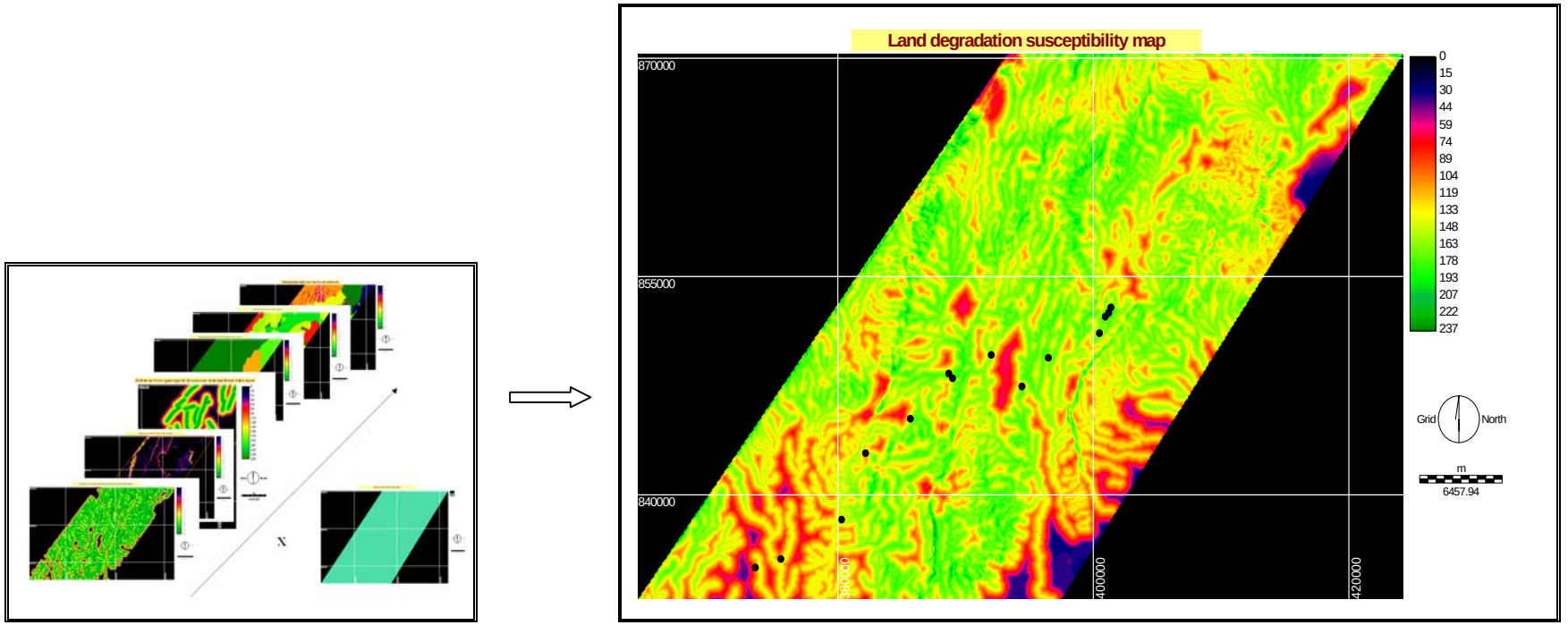

Figure 41 (a and b). Factors and constraint data layer (left) and their weighted linear combination result of Land degradation susceptibility map of the study area (factors from most to least influencing are: drainage, slope, geological structures, geology, soil and land use/ land cover) (the legend represent; high (273 and green) to low (0 and black) susceptible areas to land degradation activity) (right).

The resulting continuous land degradation susceptibility data layer (Fig. 41b) is further reclassified into three classes (Fig. 42) that divide the study area into different degrees of influenced by land degradation activity because of the existence of all the factors together in the same place and at the same time. Based on factors of drainage, slope, geological structures, lithology (geology), soil and land use/land cover of the area three classes: (Fig. 42) (class 1(green), class 2 (blue) and class 3 (yellow) representing low, moderate and high vulnerability areas to land degradation activity respectively.

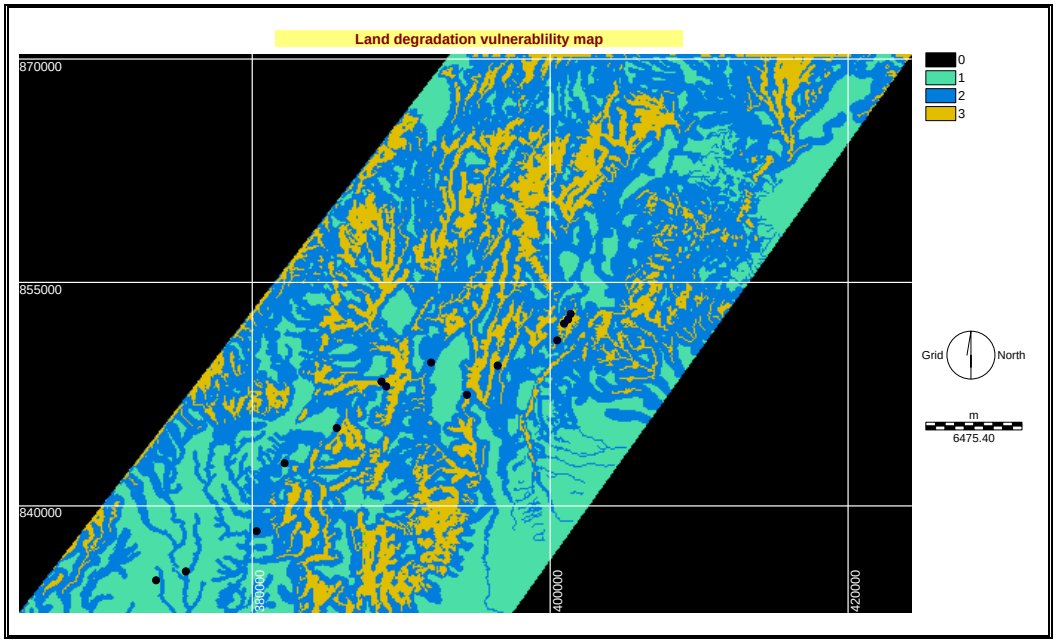

Figure 42. Land degradation vulnerability map of the study area. Class 1(green), class 2 (blue) and class 3 (yellow) represent low, moderate and highly vulnerable areas to land degradation activity respectively. Factors from most to least influencing are: drainage, slope, geological structures, geology, soil and land use/ land cover.

Anther map is produce by taking geological structures as a major factor for land degradation activity in the study area (figs. 43 – 45).

	geostructure2	slope12	ageology13	drainage3	soil41	landcover2
geostructure2	1					
slope12	0.5	1				
ageology13	0.3333	0.5	1			
drainage3	0.25	0.3333	0.5	1		
soil41	0.2	0.25	0.3333	0.5	1	
landcover2	0.1667	0.2	0.25	0.3333	0.5	1

```
The eigenvector of weights is :

   geostructure2 : 0.3825
         slope12 : 0.2504
      ageology13 : 0.1596
       drainage3 : 0.1006
          soil41 : 0.0641
      landcover2 : 0.0428



Consistency ratio =   0.02
Consistency is acceptable.
```

Figure 43. Weight of factors that control land degradation process in the study area taking geological structure data layer as a dominant factor: the pairwise ratio matrix (left), the module result of the eigenvector of ratio matrix that gives weight for each factor (right).

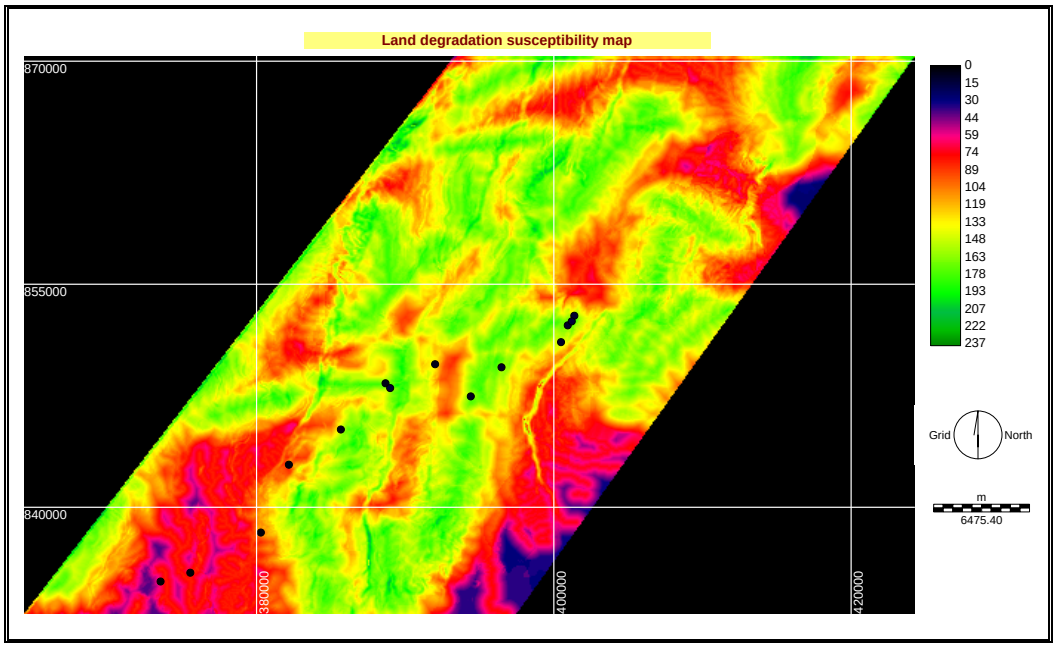

Figure 44. Land degradation susceptibility map that are taken geological structure as a dominant factor (the legend represent; high (273 and green) to low (0 and black) susceptible areas to land degradation activity). Factors from most to least influencing are: geological structures, slope, drainage, geology, soil and land use/ land cover.

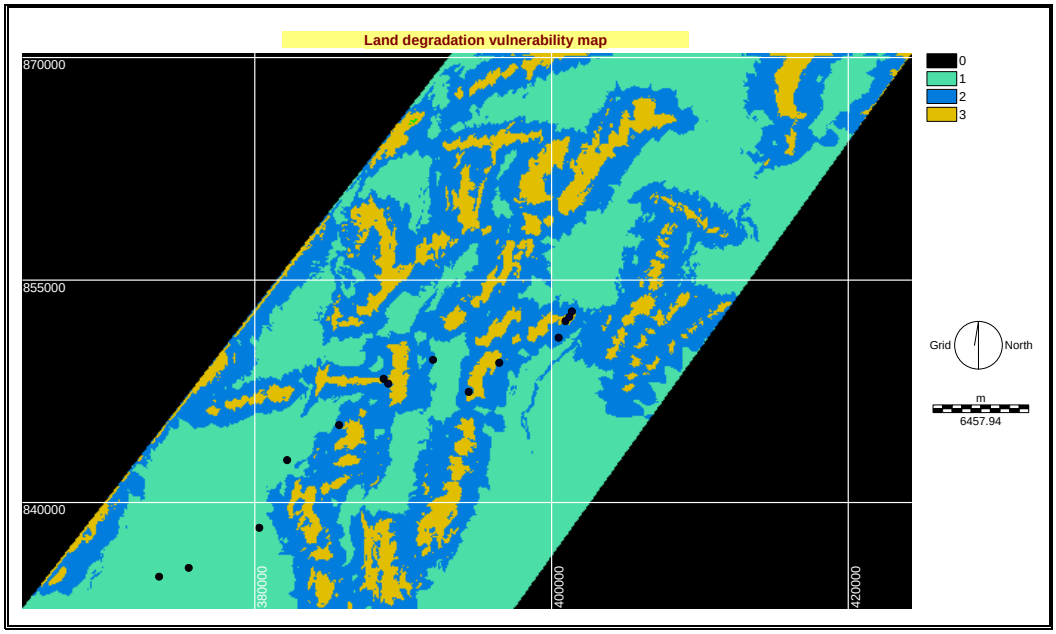

Figure 45. Land degradation vulnerability map that are taken geological structure as a dominant factor. Class 1(green), class 2 (blue) and class 3 (yellow) represent low, moderate and highly vulnerable areas to land degradation activity respectively. Factors from most to least influencing are: geological structures, slope, drainage, geology, soil and land use/ land cover.

It is observed that, the underlying geology of the study area is vulnerable or easily attacked by land degradation triggering factors because of its inherent weak nature due to this nature once land degradation activity is initiated as rills along geological structures, canals or drainage lines, they change to gullys, which in turn form inselbergs in a short period of time.

Geological structures produce high slopes, influence the direction of drainage lines that easily cut the various lithologic units and aggravate the land degradation activity.

In the study area, most rivers have developed along geological structures. Down and lateral cutting of the rivers combined with the weathering of river valley sides aggravates the land degradation process. This is mainly determined by the nature of the rock, their resistance to erosion and their structural arrangements and slope angle. Intense degradation is observed along river gorges because of differential erosion on different strata proportional to the degree of resistance of the rock layers.

7. Conclusions and recommendations

7.1. Conclusions

1. In the study area, water-driven erosion is the main land degradation process. Land degradation features are seen in the area such as sheet erosion features, rills, gullys, inselbergs and badlands.

.

2. Once land degradation activity is initiated as rills along geological structures, canals or drainage lines, they change to gullys, which in turn form inselbergs in a short period of time due to weak nature of the underlying geology.

3. In the study area at present, there is very high land degradation due to the natural vulnerability of the underlying geological material which is a sequence of different units with differential degree of resistance against erosion, and in many instances affected by faults and fractures. The loose ash fall layers, less welded tuff layers and relatively compact but weak pumice layers are highly affected by degradation. The welded and relatively strong ignimbrite is relatively more resistant; and it is more degraded where intensively fractured and when it is exposed upon removal of the weaker layers. The weakness of the underlying geological material and the existence of geological structures makes the area vulnerable to land degradation-triggering factors such as water erosion.

4. The amount of land degradation in areal base calculated on a sample site (a subset of the study area) using Landsat satellite images of the years 1973,

1984, and 2000 G. C. shows a general increasing trend. It is estimated that the amount of degraded area in the year 1973 G.C. was 7.3 %, in 1984 G. C. was 10.4 % and in 2000 G. C., it was 16.7 %.

5. The average rate of land degradation from the year 1984 to 1973 G.C. was 0.7 square kilometers per year and from the year 2000 to 1984 G.C., it was 1.0 square kilometers per year. The result shows a general increasing trend of the rate of land degradation on an areal basis.

6. Using cross tabulation pair images of the years 1984 G. C. and 1973 G. C. taken at a time, it is estimated that non degraded area in both years was 84.3 % and it decreased to 75.0 % in the pair images of the years 2000 G. C. and in 1984 G.C.

7. For multicriteria evaluation the selecting factors that control the land degradation in the study area, which from most influencing to least influencing are drainage, slope, geological structures, geology, soil, and land use/ land cover.

8. The continuous land degradation susceptibility map of the study area is reclassified into three classes of vulnerability, which are high, moderate and low vulnerable areas to land degradation activity. Based on this, areas near drainage and geological structures, on high slopes, that have lithology of ignimbrite and tuff unit, calcic xerosols soil type and land use/ land cover

types that have cultivation mixed with grassland, bush and shrub are most affected by land degradation activity.

7.2. Recommendations

1. The use of this type of remote sensing and GIS techniques is important for land degradation assessment in similar areas and this method has been used for land degradation and landslide assessments, such as (Teferi, 2005).

2. Naturally vulnerable lands to land degradation may be aggravated by man made activities and in order to reduce the land degradation activity, giving conservations priority for highly vulnerable lands is advisable.

3. Leaving the lands in order to recover naturally would be one way to reduce land degradation in the area. Reforestation can also be an appropriate measure against aggravation of land degradation process. In the study area some intensely degraded lands are leave for rehabilitation and trees are planted, and it is observed in the area that, tid is more effectively grown than eucalyptus.

4. As we see the time series analysis of land degradation, the degraded areas have a general trend of increasing over time even though the small rehabilitation activities are there. It is observed that many terraces are built in the study area mainly where land degradation is intense but they are not properly constructed and they are not strong and effective. Therefore construction of effective terraces and other engineering features using trained personnel is advisable.

8. References

Asrat, A., Barbey, P, Gleizes, G. (2001) The Precambrian Geology of Ethiopia: a review, Rock View Ltd. African Geosciences Review, 8, No 3, 271-288.

Bridges, E. M., Lal, D. H., Oldeman, L. R., Frits, W.T., Penning, Scherr, S. J., Sombatpanit, S. (2001) Response to Land Degradation, oxford press, New Delhi, 487p.

Conacher, A. J. (2001) Land degradation: papers selected from contributions to the sixth meeting of the International Geographical Unions Commission on Land Degradation and Desertification, Perth, Western Australia, 20 – 28 September 1999, GeoJournal Library series, 58, 400p.

CSA (central statistical Authority) (1996) Federal democratic republic of Ethiopia office of population and housing census commission, The 1994 population and housing census of Ethiopia results for southern nations, nationalities and peoples' region, 1:part 1. June 1996, Addis Ababa.

Eswaran, H., Lal, R., Reich, P.F. (2001) Land degradation: An Overview, 20 – 35.

Eastman, J.R. (2001) IDRISI 32 release 2: Guide to GIS and Image Processing, 2, Manual Version 32.20, Clark Labs, Clark university (1987 – 2001).

FAO (1994) in Apisit Eiumnoh, Tools for identification, assessment and monitoring of land degradation, 248 – 259p.

Lillesand, T. M., Kiefer R. W. (2000), Remote Sensing and Image Interpretation, 4th Edition, John Wiley & Sons, Inc., New York, 715p.

Mahatsente, R., Jentzsch, R. G., Jahr, T. (1999), Crustal structure of the main Ethiopian rift from gravity data: 3–dimensional modeling. Tectonophysics 313, 363 – 382.

Malczewski, J (1999) GIS and multicriteria decision analysis, John Wiley & sons, New York, 392p.

Monkhouse, F. J. (1975) Principles of Physical Geography. Hodder & Stoughton, Newcastle upon Tyne, 570p.

Nyssen, J., Pooesen, J., Moeyersons, J., Deckers, J., Haile M., Lang, A. (2004) Human Impact on the Environment in the Ethiopian an Eritrean Highlands-A State of the Art. Earth Science reviews, 64, 273-320.

Reich, P.F., Numbem, S.T., Almaraz, R.A., Eswaran, H (2001) Land resource stresses and desertification in Africa, oxford press, New Delhi, 101 – 114.

Sagari, M. (1998), environmental changes analysis and their applications to agriculture in the Lake Region (Ethiopia), land resources inventory, 183p.

Taddese, G. (2001) Land Degradation: A Challenge to Ethiopia. Environmental Management, 27, 818 – 824.

Tadesse, S., Milesi, J.P., Deschamps, Y., Ralay, F., Heinry, C., Chene, F., (2004) Geology and Mineral map of Ethiopia,

Teferi, Y. (2005) Evaluation of land degradation and land slide using integrated remote sensing and GIS approach around Wolayita Sodo-Shone area, south Ethiopia. Master Thesis, Addis Ababa University, Ethiopia, 147p.

Tekle, K. (1999) Land degradation Problems and their Implication for food shortage in south Wollo, Ethiopia: a Forum. Environmental management, 23, 419 – 427p.

Warren, A., Agnew C. (1988) An assessment of desertification and land degradation in arid and semi-arid areas. International Institute for Environment and Development (IIED) paper no. 2. London: Ecology and Conservation Unit, University College.

WoldeGabriel, G., Aronson, J.L., Walter, R. C. (1990) Geology, geochronology, and rift basin development in the central sector of the Main Ethiopian Rift. Geological Society of America Bulletin, 102, 439-458.

Woody Biomass (2001) Woody Biomass Inventory and Strategic Planning Project, Southern Nations, Nationalities and Peoples' region: Report on natural grazing lands and livestock feed resources, 102p.

Internet sources

FAO, AGL (2000), Management of degraded soils in southern and east Africa (MADS – SEA – Network). http://www.fao.org/ag/agl/agll/madssea/intro.htm

Ramirez, E (2006), Shuttle Radar Topographic Mission (SRTM), the mission to map the world. Jet propulsion laboratory, California. http://www.jpl.nasa.gov/srtm

UNEP (1999) Global Environment Outlook - 2000. United Nations Environment Programme. Earthscan Publications, London. http://www.unep.org/geo2000

Office of Arid Lands Studies (2001) FAO /UNESCO system of soil classification http://ag.arizona.edu/OALS/soils/fao.html